Response to Referee #1 (Dr. Rodney Weber)

This paper assesses the composition of $PM_{2.5}$ in Seoul under different transport & meteorological conditions. The separation of data collection into periods when Seoul was impacted or not by upwind transport from China, combined with local ventilation conditions over Seoul, is clever and insightful. The result is that clear differences in the aerosol composition and processes can be identified. The authors show that highest $PM_{2.5}$ concentrations occur when species transported from China are present and when there is little dispersion over Seoul, as might be expected. The unique feature is they find that these periods have enhanced inorganic aerosol concentrations and investigate a number of possible feedbacks that could explain the enhanced aerosol concentrations under these conditions, all related to aerosol liquid water levels (ALW). This includes enhanced SO_2 oxidation to form sulfate and especially the uptake of HNO_3 to form particle NO_3^-. The specific contributions of China (SO_2 / sulfate) vs Seoul (NO_x / NH_3) on these interactions is also identified. This allows a unique assessment of possible control strategies to reduce $PM_{2.5}$ mass. The main issue with this paper is the lack of NH_3 and HNO_3 data that are required to run the thermodynamic model. The authors should more fully assess this limitation through a detailed sensitivity analysis, but my suspicion is it will not significantly change the result.

We appreciate the reviewer for valuable comments and suggestions. As indicated in the following point-by-point responses, we have incorporated the reviewer's comments and suggestions into the revised manuscript. We have conducted additional analyses, modified texts, figures, and tables, and added several new figures (Figs. 4 and 5) and references in the revised version. Each response to the reviewer is in blue, and the change in the manuscript is in red.

During the revision process, we found that the molar concentrations of Ca^{2+} and Mg^{2+} in the ISORROPIA input data were mistakenly applied by 2-time values. We have corrected those input data errors and newly conducted simulations. As a result, average and standard deviation of ALW (both W_i and W_o), ionic strength, pH, oxidation/partitioning ratios [SOR, $\varepsilon(NO_3^-)$, and $\varepsilon(NH_4^+)$] in Table 2 have been slightly changed. By the changes in results, several figures (Figs. 6a, g, and h, Fig 7, Fig. 8, Fig. 10, and Fig. 11 in the revised version) have also been modified. However, such changes are negligible and did not affect our conclusions.

We also corrected average and standard deviation of NH_3 concentrations in Table 2, because the unit of original version were μg m^{-3}. NH_3 are now represented by unit of ppb in the revised version. Sect. 2.2 and Sect. 2.3 were exchanged with each other to keep consistency of the order of figures and text contents.

Specific Comments:

The use of acronyms made the paper, at times, difficult to follow for me. Where it is possible, it might be better to just write out the term. A list (table) defining them could also be useful. For example, in this study SIA is just sulfate, nitrate and ammonium.

Thanks for the comment. We tried to reduce the usage of acronyms in the revised version.

Potential NO_3^- sampling issues? Were samples gas denuded; seems not but maybe use of Teflon filters minimizes this possible positive artifact? Since particle NO_3^- is a large component of this paper, and it is known to be difficult to measure using filters due to evaporation, this issue should be discussed. That is, is it possible that ammonium nitrate is significantly under-measuring in this study?

As the reviewer pointed out, we did not employ both a denuder and backup filters for $PM_{2.5}$ sampling on Teflon filters. Therefore, there are possibilities of both positive and negative artifacts by absorption of gas-phase nitric acid on the filter and evaporation of ammonium nitrate. Although both artifacts may partly compensate each other, previous evaluation studies showed that the major concern of nitrate measurement on Teflon filter is the negative artifact (Ashbaugh and Eldred, 2004; Chow et al., 2005). Nie et al. (2010) reported large nitrate loss (~75%) at the lower nitrate concentrations (< 10 μg m^{-3}) but much smaller nitrate loss (~10%) at the higher nitrate concentrations (> 10 μg m^{-3}) attributable to formation of particle cake, even in summertime (temperature range of 22–34°C) in Beijing. Considering that the evaporative loss of nitrate was minimal in winter, they expected small to moderate sampling artifacts for conventional sampling method (un-denuded filter sampling without backup filters) in polluted eastern China.

In this study, average temperature of two *regional transport* (V-T and S-T) groups are much lower than summer (~9°C), and average nitrate concentrations of these two groups are high (> 10 μg m^{-3}). In addition, although average nitrate concentrations of the *local ventilation with no regional transport* (V-nT) group are very low (~2 μg m^{-3}), the cold temperature (~3°C) can prevent evaporation of ammonium nitrate from the Teflon filter. Therefore, we expected potential nitrate loss for these three groups to be small enough (< 20%). The *local stagnation with no regional transport* (S-nT) group is probably most affected by evaporation because of its low nitrate concentration (~5 μg m^{-3}) with moderate temperature (~15°C). However, nitrate loss of this group would not be as much as that of the summertime Beijing (~75%) reported by Nie et al. (2010).

We further examined the sensitivity of our results by potential negative artifacts in NO_3^- through the ISORROPIA simulations using hypothetical NH_4^+ and NO_3^- concentrations considering evaporative nitrate loss [from 0% (no loss) to 80% loss of ammonium nitrate from the filter samples] together with the average concentrations of $PM_{2.5}$ components for each categorized group summarized in Table 2 (Fig. S8). Note that the results from the 0% nitrate loss assumption do not exactly same as the values in Table 2, because Table 2 shows the average of measured and predicted data for each group while Fig. S8 is obtained from the simulations using the average inorganic concentrations. If we assumed a 20% nitrate loss [NO_3^- and excess $NH_4^+ = (NH_4^+ / SO_4^{2-} - 1.5) \times SO_4^{2-}$; Pathak et al., 2004] for the V-nT, V-T, and S-T groups and a 50% nitrate loss for the S-nT group based on above discussion, the nitrate fraction in $PM_{2.5\,dry}$ of the S-nT group becomes comparable to that of the *regional transport* (V-T and S-T) groups (Fig. S8a). However, inorganic ALW (W_i), $\varepsilon(NO_3^-)$, and $\varepsilon(NH_4^+)$ of the V-T and S-T groups are still larger than that of the S-nT group (Figs. S8b, d, and e), and this supports an important role of the transported wet particles in the formation of $PM_{2.5}$ inorganic species. In conclusion, therefore, potential negative artifacts induced by the un-denuded filter sampling method without backup filters do not significantly change the conclusions of this study.

To clarify the effect of potential errors from the sampling artifacts on our results, we added the following paragraph to the end of Line 90 on page 3 (as the third paragraph in Sect. 2.1).

Note that the $PM_{2.5}$ sampling on Teflon filter for inorganic ions was conducted without both a denuder and backup filters, and thus there could be potential sampling artifacts on the results, particularly negative artifacts in semivolatile ammonium nitrate (Ashbaugh and Eldred, 2004; Chow et al., 2005). Nie et al. (2010) reported that summertime nitrate loss on Teflon filter from the un-denuded filter sampling without backup filters is to be ~75% at lower nitrate concentrations (< 10 μg m^{-3}) but only ~10% at higher nitrate concentrations (> 10 μg m^{-3}) due to the formation of particle cake. Considering small evaporative loss in the cold season and the high nitrate concentration in Seoul, we expected small to moderate sampling errors in this study. Sensitivity tests considering potential ammonium nitrate loss from the filter samples show that the assumption of 20% nitrate loss for the high concentrations with low-temperature groups and 50% nitrate loss for the low concentrations with moderate temperature group does not change our conclusion (Fig. S8).

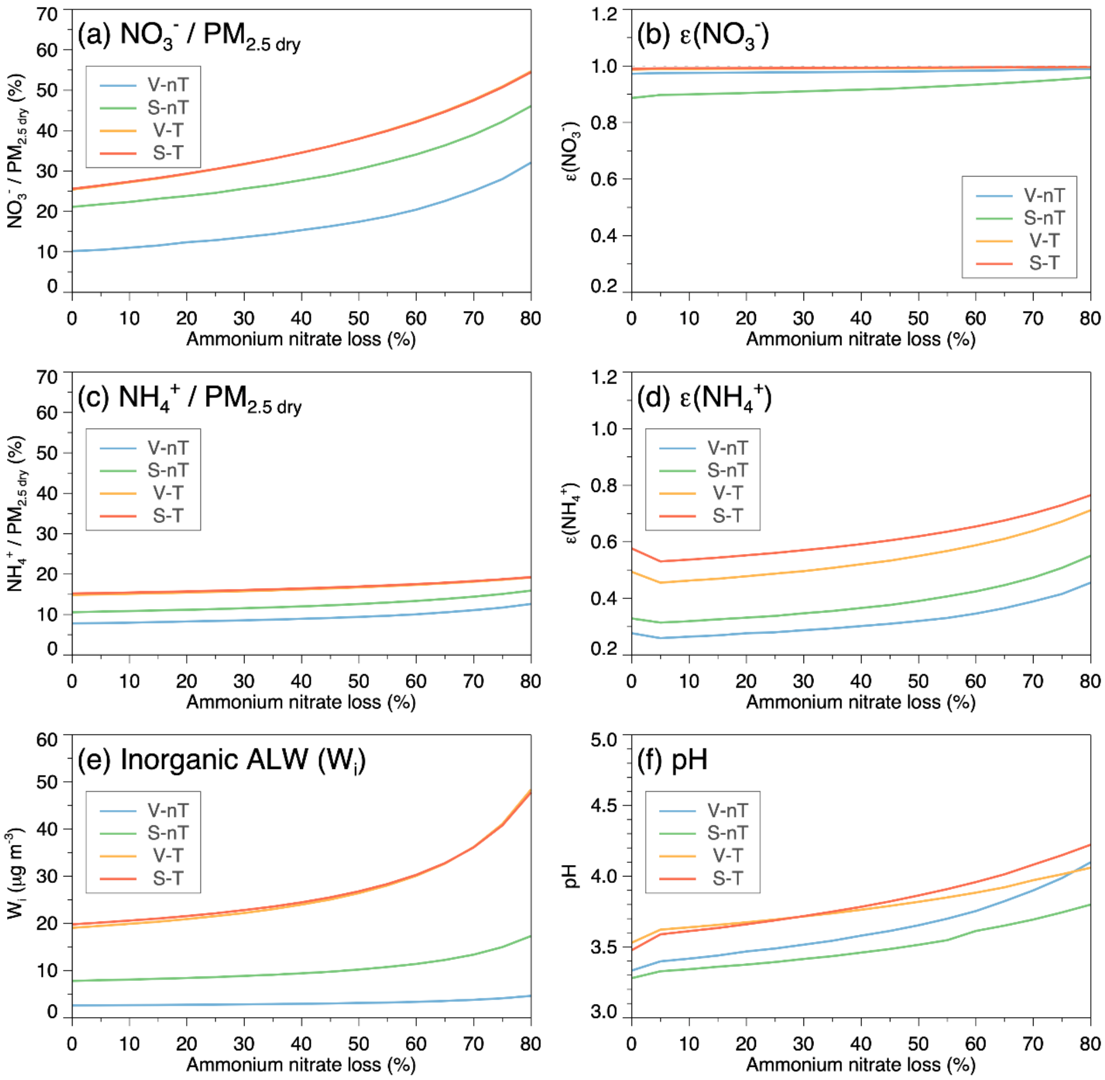

Figure S8: Sensitivity of (a) nitrate fraction in dry $PM_{2.5}$ (NO_3^- / $PM_{2.5\ dry}$), (b) nitrate partitioning ratio [$\varepsilon(NO_3^-)$], (c) ammonium fraction in dry $PM_{2.5}$ (NH_4^+ / $PM_{2.5}$), (d) ammonium partitioning ratio [$\varepsilon(NH_4^+)$], (e) inorganic ALW (W_i) content, and (f) pH to the hypothetical ammonium nitrate loss during the sampling on Teflon filters. Average $PM_{2.5}$ components (Table 2) with extrapolated concentrations of NO_3^- and excess NH_4^+ [$NH_4^+{}_{excess} = (NH_4^+ / SO_4^{2-} - 1.5) \times SO_4^{2-}$; Pathak et al., 2004], considering the hypothetical ammonium nitrate loss from 0% to 80%, were employed in the ISORROPIA simulations. Sensitivity curves in blue, green, yellow, and red colors represent the *local ventilation with no regional transport* (V-nT) group, *local stagnation with no regional transport* (S-nT) group, *local ventilation with regional transport* (V-T) group, and *local stagnation with regional transport* (S-T) group, respectively.

Ashbaugh, L. L. and Eldred R. A.: Loss of particle nitrate from Teflon sampling filters: Effects on measured gravimetric mass in California and in the IMPROVE network, J. Air Waste Manage. Assoc., 54, 93–104, https://doi.org/10.1080/10473289.2004.10470878, 2004.

Chow, J. C., Watson, J. G., Lowenthal, D. H., and Magliano, K. L.: Loss of $PM_{2.5}$ nitrate from filter samples in central California, J. Air Waste Manage. Assoc., 55, 1158–1168, https://doi.org/10.1080/10473289.2005.10464704, 2005.

Nie, W., Wang, T., Gao, X., Pathak, R. K., Wang, X., Gao, R., Zhang, Q., Yang, L., and Wang, W.: Comparison among filter-based, impactor-based and continuous techniques for measuring atmospheric fine sulfate and nitrate, Atmos. Environ., 44, 4396–4403, https://doi.org/10.1016/j.atmosenv.2010.07.047, 2010.

Pathak, R. K., Yao, X., and Chan, C. K.: Sampling artifacts of acidity and ionic species in $PM_{2.5}$, Environ. Sci. Technol., 38, 254–259, https://doi.org/10.1021/es0342244, 2004.

Regarding the estimated NH_3 and effect on pH. A sensitivity test is warranted, as noted by another reviewer. This could include discussing $\varepsilon(NH_4^+)$ and $\varepsilon(NO_3^-)$. Table 2 suggests that with $\varepsilon(NH_4^+)$ values ranging from 0.23 to 0.5, there may be some sensitivity to $[NH_3]$. But as noted, this may not contribute to much change in pH. Furthermore given Fig 9, in some situations this may not have a large effect on predicted NO_3^-. The point is, the epsilon data for NH_4^+ and NO_3^- can be used to help assess the sensitivity of the predictions to uncertainties in gas phase species that were not measured; eg, one could make a graph of $\varepsilon(NH_4^+)$ similar to Fig 9 and then show the data for a range of estimated NH_3 and HNO_3 around the predicted values.

Following the reviewer's suggestion, we conducted sensitivity tests for pH and inorganic partitioning ratios $[\varepsilon(NO_3^-)$ and $\varepsilon(NH_4^+)]$ and represented the results as Fig. 5 in the revised version. As the reviewer expected, the changes in pH, $\varepsilon(NO_3^-)$, and $\varepsilon(NH_4^+)$ by NH_3 is not significant when NH_3 concentration is larger than 5 ppb.

Various NH_3 levels from 0 ppb to 50 ppb are applied for all the measurement days as fixed values (no day-to-day variations in NH_3) in our sensitivity tests. Figs. 5a, c, and e show good correlations between the results from simulation with daily varied NH_3 (average of 10.9 ppb) and that with daily fixed NH_3 if it was not 0 ppb. This indicates that the potential errors in pH and partitioning ratios from the day-to-day estimation seem to be limited. Figs. 5b, d, and f show that the average pH and partitioning ratios for each categorized group become flattened over the 5 ppb of NH_3. Therefore, the potential errors from the estimation of NH_3 do not change our conclusion.

We added the content related to the sensitivity test for NH_3 to Line 130 on page 5 of the original manuscript as follows:

We conducted ISORROPIA simulations with various NH_3 levels (0–50 ppb) applied for all the measurement days as fixed values to further explore the sensitivity of pH, $\varepsilon(NO_3^-)$, and $\varepsilon(NH_4^+)$ to NH_3. Good correlations between results from the daily varied NH_3-simulation and the fixed NH_3-simulations shows that potential errors induced by the estimation of daily NH_3 levels will be small if NH_3 concentrations are nonzero (Figs. 5a, c, and e). Increasing pH and $\varepsilon(NO_3^-)$ and decreasing $\varepsilon(NH_4^+)$ by the increase in fixed NH_3 level become flatten over the range from a half to 2 times of the average NH_3 concentration in Seoul (~5–20 ppb; Phan et al., 2013) (Figs. 5b, d, and f), and this indicates that the potential errors in reconstructed NH_3 will not significantly change the results in this study.

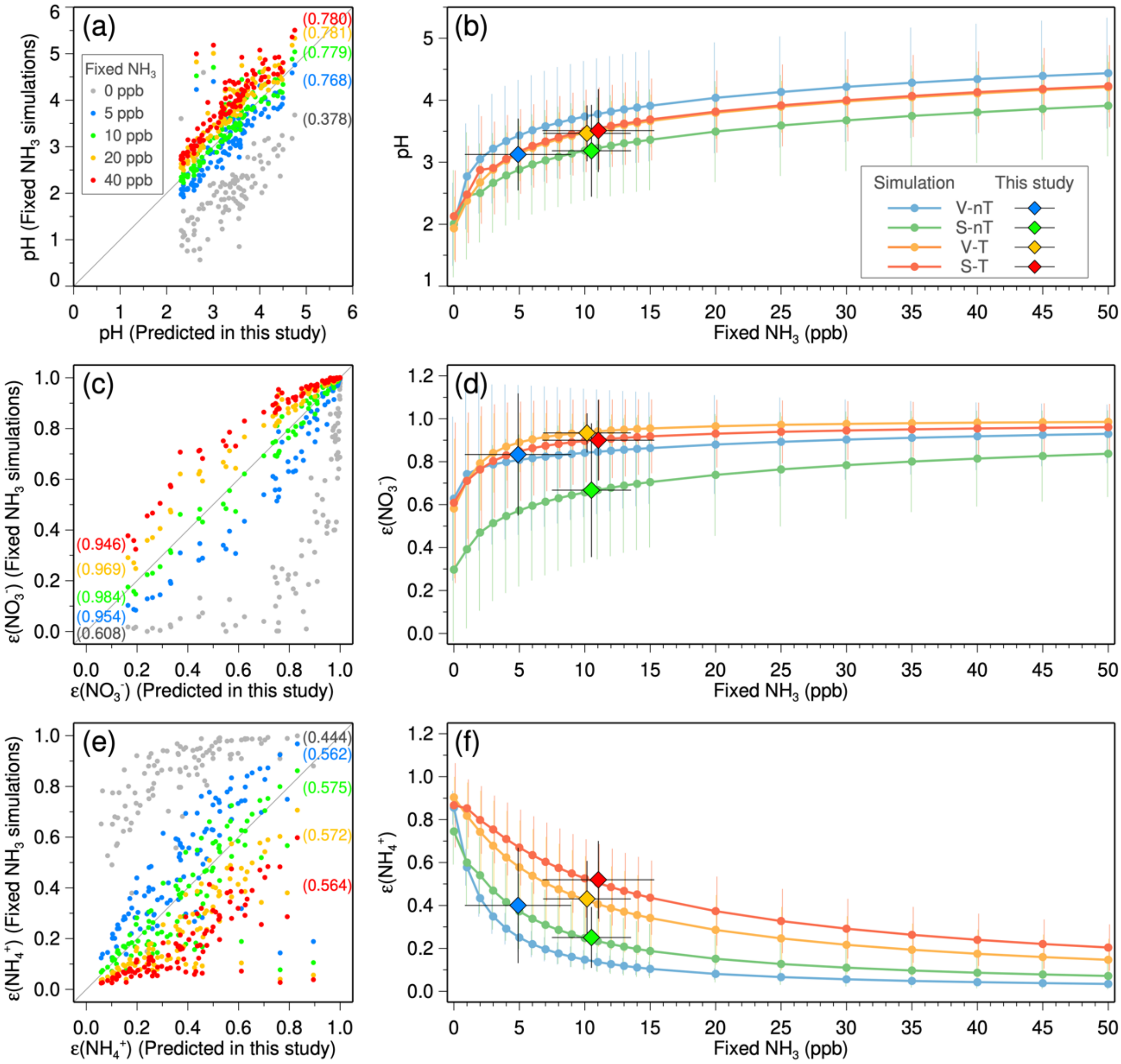

Figure 5: Sensitivity of (a–b) predicted pH, (c–d) nitrate partitioning ratio [$\varepsilon(NO_3^-) = NO_3^- / (HNO_3 + NO_3^-)$], and (e–f) ammonium partitioning ratio [$\varepsilon(NH_4^+) = NH_4^+ / (NH_3 + NH_4^+)$] to gas-phase ammonia ($NH_3$) concentrations. (a, c, and e) Comparisons between the simulation in this study (using the daily reconstructed NH_3 concentrations) and the simulations with the various fixed NH_3 levels (colored dots in gray, blue, green, yellow, and red for 0 ppb, 5 ppb, 10 ppb, 20 ppb, and 40 ppb, respectively). Values in round brackets are the R-squared values of the linear regressions. Gray solid lines indicate a 1-to-1 relationship. (b, d, and f) Average (solid circles) and standard deviation (vertical bars) of pH, $\varepsilon(NO_3^-)$, and $\varepsilon(NH_4^+)$ for the *local ventilation with no regional transport* (V-nT) group (light blue), *local stagnation with no regional transport* (S-nT) group (light green), *local ventilation with regional transport* (V-T) group (light yellow), and *local stagnation with regional transport* (S-T) group (light red) with respect to the various fixed NH_3 levels from 0 ppb to 50 ppb. Averages and standard deviations of the reconstructed NH_3 concentrations and obtained pH, $\varepsilon(NO_3^-)$, and $\varepsilon(NH_4^+)$ for the V-nT, S-nT, V-T, and S-T groups are represented as blue, green, yellow, and red diamonds with horizontal and vertical bars.

Line 319, one could be more specific here, with $\varepsilon(NO_3^-)$ near or at 1 there is a direct relation between NO_x control and particle NO_3^-.

We added following sentence behind the line 319:

Such a direct relationship between NO_x control and nitrate aerosol is significant at the condition of $\varepsilon(NO_3^-)$ close to 1.

Sulfate is a large component of the SIA. How does sulfate play a role in this feedback mechanism (see next)?

The idea of feedback (or sometimes called co-condensation) leading to more uptake of NH_3 and HNO_3 by the added liquid water is not a new concept. I suggest the authors think about it some more and add a deeper discussion. It happens for any semi-volatile acidic species that when partitioned to the particle phase significantly increases the water uptake, which then raises the pH and allows more uptake. Examples include HCl / Cl^- & HNO_3 / NO_3^-. Since sulfate is not semi-volatile and highly hygroscopic the semivolatile species involved that is driving this feedback process must generally have significantly higher concentrations then sulfate, or more precisely, contribute comparable or more to AWC than sulfate, otherwise the feedback does not exist. For example, in this study if sulfate was significantly larger then nitrate, would nitrate levels increase due to uptake of water? Probably not because sulfate would then control the overall AWC. One could play around with sulfate concentrations to see when this happens. The process discussed here is very similar to that discussed in Guo et al. (2017). Also, as another example, see Topping et al (2013).

Guo, H., J. Liu, K. D. Froyd, J. Roberts, P. R. Veres, P. L. Hayes, J. L. Jimenez, A. Nenes, and R. J. Weber (2017), Fine particle pH and gas-particle phase partitioning of inorganics in Pasadena, California, during the 2010 CalNex campaign, Atm. Chem. Phys., 17, 5703–5719.

Topping, D., P. Connolly, and G. McFiggans (2013), Cloud droplet number enhanced by co-condensation of organic vapours, Nature Geoscience, 6, 443–446.

We appreciate the reviewer's comment and suggestion on this. As the reviewer pointed out, the significant nitrate concentration compared to sulfate can promote the feedback mechanism including water and nitrate uptake into the particle together with pH increase. This relationship can be also found in our results. For example, the nitrate-to-sulfate molar ratio is largest in the *local stagnation with regional transport* (S-T) group (1.87), followed by the *local ventilation with regional transport* (V-T) group (1.60), the *local stagnation with no regional transport* (S-nT) group (1.29), and the *local ventilation with no regional transport* (V-nT) group (0.81). Because inorganic ALW, pH, and $\varepsilon(NO_3^-)$ are high in the *regional transport* (V-T and S-T) groups followed by the S-nT and V-nT groups (Table 2), this feedback process explains the synergistic effect of transported (wet) particle on the nitrate uptake.

We added the content related to the feedback mechanism to Line 285 on page 9 of the original manuscript as follows:

In terms of the synergistic increase in NO_3^- with ALW, the ratio between NO_3^- and SO_4^{2-} can be an important factor. Hygroscopic uptake of ALW by both SO_4^{2-} and NO_3^- can increase pH by dilution effect on hydrogen ions. Because NO_3^- is a semi-volatile hygroscopic species, the higher pH increased by ALW allows more partitioning of HNO_3 gas into the particle phase, and uptake more ALW. However, if SO_4^{2-} is dominant in the particle, such a feedback process will be weakened because sulfate is non-volatile (Guo et al., 2017). The average nitrate-to-sulfate molar ratios of the *regional transport* groups (1.87 for the S-T group and 1.60 for the V-T group) are higher than that of the no regional transport groups (1.29 for the S-nT group and 0.81 for the V-nT group). Since ALW, pH, and $\varepsilon(NO_3^-)$ in the *regional transport* (V-T and S-T) groups are higher than those in the *no regional transport* (V-nT and S-nT) groups, this feedback process can explain the synergistic effect of transported particle on high NO_3^- and ALW fractions.

Response to Referee #2

General comments:

Seo et al. combined measurements of $PM_{2.5}$ mass and composition (from filter collection) in Seoul, Korea, with thermodynamic modeling in ISORROPIA II and back trajectory analysis. They find that particles influenced by regional transport from source areas in China have higher mass, higher inorganic aerosol content and higher water content. Specifically, the highest concentrations are observed in air masses under locally stagnant conditions affected by regional transport. They conclude that the synergistic effects of local stagnation and regional transport affect $PM_{2.5}$ concentrations and composition.

Except for a few English usage issues, the manuscript is well written and within the scope of Atmospheric Chemistry and Physics. While the measurements are local, the main conclusion(s) are likely applicable to other regions and are therefore of broader interest. I have one major and several minor comments and concerns which should be addressed before publication.

We appreciate the reviewer for careful reading and helpful comments that improve our manuscript. As indicated in the following point-by-point responses, we have incorporated the reviewer's comments and suggestions into the revised manuscript. We have conducted additional analyses, modified texts, figures, and tables, and added several new figures and references in the revised version of manuscript. Each response to the reviewer is in blue, and the change in the manuscript is in red.

During the revision process, we found that the molar concentrations of Ca^{2+} and Mg^{2+} in the ISORROPIA input data were mistakenly applied by 2-time values. We have corrected those input data errors and newly conducted simulations. As a result, average and standard deviation of ALW (both W_i and W_o), ionic strength, pH, oxidation/partitioning ratios [SOR, $\varepsilon(NO_3^-)$, and $\varepsilon(NH_4^+)$] in Table 2 have been slightly changed. By the changes in results, several figures (Figs. 6a, g, and h, Fig 7, Fig. 8, Fig. 10, and Fig. 11 in the revised version) have also been modified. However, such changes are negligible and did not affect our conclusions.

We also corrected average and standard deviation of NH_3 concentrations in Table 2, because the unit of original version were $\mu g\ m^{-3}$. NH_3 are now represented by unit of ppb in the revised version. Sect. 2.2 and Sect. 2.3 were exchanged with each other to keep consistency of the order of figures and text contents.

Major comments:

In section 2.2, the author describes reconstructing concentrations of HNO_3 and NH_3 for their thermodynamic modeling analysis. I have two main issues with this:

1. In my opinion, the current version of the manuscript does not sufficiently justify the methods of reconstruction. For NH_3, the authors seem to assume that the concentrations at the Gwangjin site are the same as the concentrations at the KIST site, and that they did not change between years. Please describe why these are reasonable assumptions.

Since there were no NH_3 measurements in Seoul for the analysis period of 2012–2014, we had to reconstruct NH_3 concentrations for the thermodynamic model simulations in some way. Fortunately, we found a year-long measurement (2010–2011) of NH_3 at the Gwangjin site (37.545°N, 127.096°E, 7.8 km southeastward away from the KIST site) in Seoul reported by Phan et al. (2013). Although the NH_3 data reported by Phan et al. (2013) has some spatiotemporal gaps (~1 to 3 years) to data in this study measured at the KIST site (37.603°N, 127.047°E), we assumed that both two site data shares statistical characteristics like annual average NH_3 level, standard deviation, and correlations with meteorological factors (temperature, RH, and wind speed) and anthropogenic gas pollutants (SO_2, NO_2, and CO), as mentioned in Text S1. Our assumption is based on (i) the small interannual changes in the estimated NH_3 emissions in Seoul from the Clean Air Policy Support System (CAPSS) inventory (Lee et al., 2011; NIER, 2018) (Fig. S5) and (ii) the similar environment of both two sites that are located downwind of the downtown core in the prevailing westerlies in Seoul and surrounded mainly by residential areas and small urban green areas (modified version of Fig. S1).

To clarify the justification of the NH_3 reconstruction based on the data by Phan et al. (2013), we added the following sentences to the end of Line 111 on page 4 of the original version as follows:

There were small interannual changes in the estimated NH_3 emission in Seoul (Fig. S5; NIER, 2018), and both two sites share similar environments located downwind from the downtown core under the prevailing westerlies and surrounded by residential and small urban green areas (Fig. S1). Therefore, we assumed that the statistical characteristics of both two sites and periods would be similar despite the temporal gap (~1–3 yr) and spatial distance (~7.8 km) between this study and Phan et al. (2013).

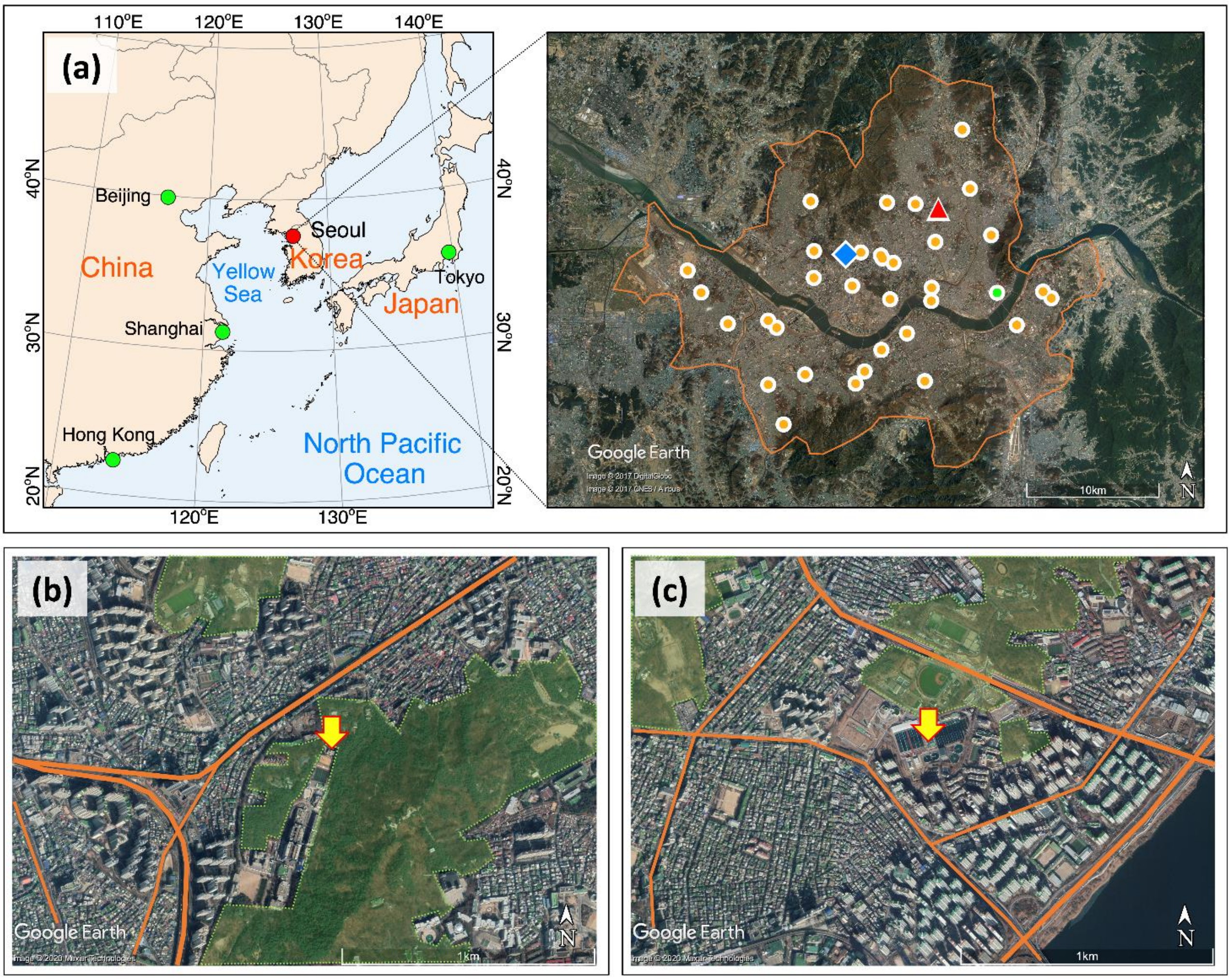

Figure S1: (a) The locations of Seoul (left panel) and the Korea Institute of Science and Technology (KIST) $PM_{2.5}$ sampling site (red triangle), the Korea Meteorological Administration (KMA) weather station (blue diamond), and Korea Ministry of Environment (KMOE) air quality monitoring sites (34 solid circles in yellow and green) in Seoul (right panel). The solid circle in green indicates the Gwangjin site at which a year-long NH_3 measurement was conducted by Phan et al. (2013). (b–c) Satellite maps of (b) the KIST $PM_{2.5}$ sampling site (37.603°N, 127.047°E) utilized in this study and (c) the Gwangjin site (37.545°N, 127.096°E) for NH_3 measurement in Phan et al. (2013). Yellow arrows are the sampling locations, areas shaded by light green are urban green areas, and lines in orange are the main roads. The background satellite images are courtesy of Google Earth.

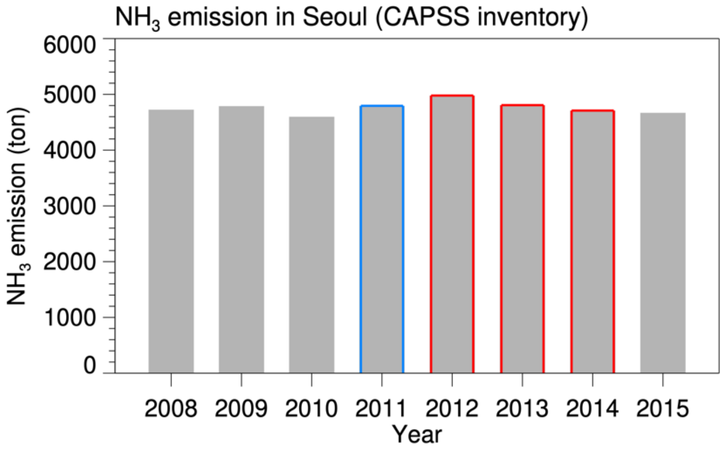

Figure S5: Estimated annual NH_3 emissions in Seoul for 2008–2015 from the Clean Air Policy Support System (CAPSS) inventory (NIER, 2018).

Lee, D.-G., Lee, Y.-M., Jang, K., Yoo, C., Kang, K., Lee, J.- H., Jung, S., Park, J., Lee, S.-B., Han, J., Hong, J., and Lee, S.: Korean national emissions inventory system and 2007 air pollutant emissions, Asian J. Atmos. Environ., 5, 278–291, https://doi.org/10.5572/ajae.2011.5.4.278, 2011.

NIER (National Institute of Environmental Research): National air pollutants emission 2015 (NIER-GP2017-210), NIER, Incheon, South Korea, available at: http://webbook.me.go.kr/DLi-File/NIER/09/023/5668670.pdf (last access: 21 October 2019), 2018 (in Korean).

For HNO_3, the authors seem to assume that the NO_3/HNO_3 ratio does not depend on the sum of NO_3+HNO_3 concentrations. Please justify this assumption.

In general, the NO_3^- / HNO_3 ratio depends on temperature, aerosol liquid water (ALW), and pH. Among these three variables, temperature is an independent meteorological variable, and ALW is dependent on the sum of salts and relative humidity. Therefore, the NO_3^- / HNO_3 ratio obtained from the simulation with reconstructed NH_3 (Simulation 2 in Fig. 4 in the revised manuscript) can be changed solely by the potential changes in pH owing to the increase in total HNO_3 (from NO_3^- to NO_3^- + HNO_3). In the NH_3-rich condition like Seoul, the potential changes in pH can be small due to the buffering effect of NH_3 partitioning (Weber et al., 2016). Therefore, we can use the NO_3^- / HNO_3 ratio from Simulation 2 and the measured NO_3^- to estimate the total HNO_3. Fig. 4 shows comparisons of pH, $\varepsilon(NO_3^-)$, and $\varepsilon(NH_4^+)$ among three simulations (Simulation 1 with only ions, Simulation 2 with ions and reconstructed NH_3, and Simulation 3 with ions, reconstructed NH_3, and HNO_3 estimated by the NO_3^- / HNO_3 ratio from Simulation 2), and here we can see that the pH is largely changed by the introduction of NH_3 gas but is nearly not changed by the increase in total HNO_3.

To justify the estimation of HNO_3 by using the NO_3^- / HNO_3 ratio, we added the following sentences to Line 119 on page 4 of the original version as follows:

Note that we regarded the HNO_3 / NO_3^- ratio as approximately independent of the total HNO_3. Although the nitrate partitioning depends on temperature, ALW content, and pH in general, the HNO_3 / NO_3^- ratio is affected alone by pH because both temperature and ALW are independent variables in this step. In the existence of excess NH_3 as we assumed for Seoul (~10 ppb at the first step), changes in pH by total HNO_3 are limited owing to the buffering effect of NH_3–NH_4^+ partitioning (Weber et al., 2016; Guo et al., 2018; Lim et al., 2020). The pH, nitrate partitioning ratio [$\varepsilon(NO_3^-) = NO_3^- / (HNO_3 + NO_3^-)$], and ammonium partitioning ratio [$\varepsilon(NH_4^+) = NH_4^+ / (NH_3 + NH_4^+)$] from the ISORROPIA simulations with and without gas-phase HNO_3 information show negligible differences between each other (Figs. 4d–f), unlike the significant role of additional NH_3 information on increasing pH and $\varepsilon(NO_3^-)$ and decreasing $\varepsilon(NH_4^+)$ (Figs. 4a–c).

Also, we added Fig. 4 into the manuscript in the revised version.

Simulation 2 (with estimated NH_3 gas) vs. Simulation 1 (without NH_3 and HNO_3 information)

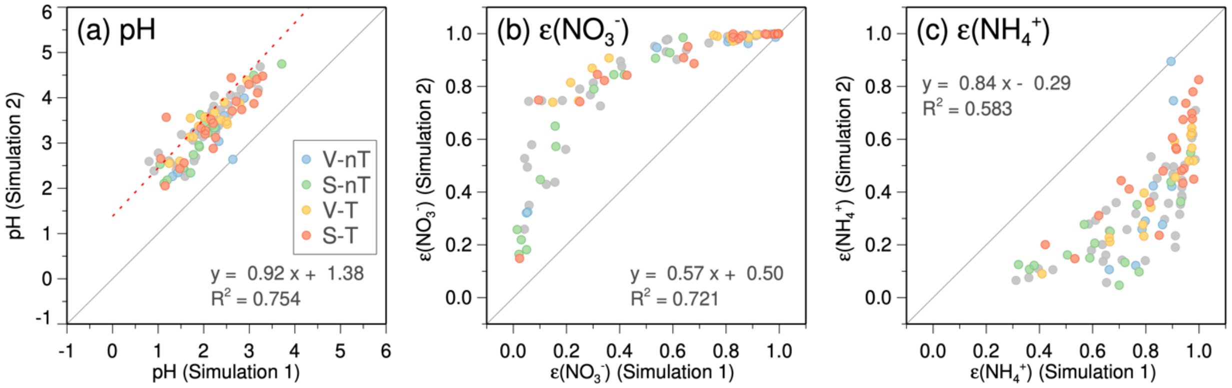

Simulation 3 (with both estimated NH_3 and HNO_3 gases) vs. Simulation 2

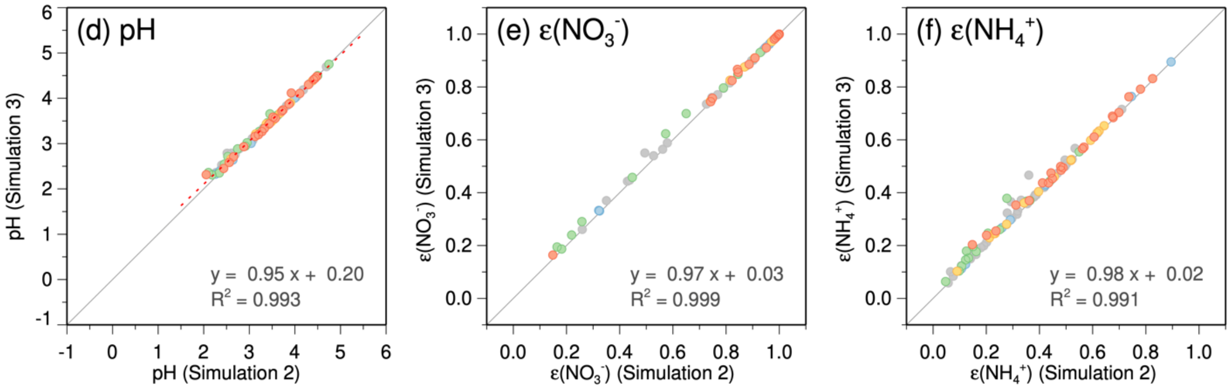

Figure 4: Comparisons of the predicted pH, nitrate partitioning ratio [$\varepsilon(NO_3^-) = NO_3^- / (HNO_3 + NO_3^-)$], and ammonium partitioning ratio [$\varepsilon(NH_4^+) = NH_4^+ / (NH_3 + NH_4^+)$] between (a–c) the simulation without gas-phase NH_3 and HNO_3 information (using NH_4^+ and NO_3^- as the total NH_3 and total HNO_3; Simulation 1) and the simulation with reconstructed NH_3 (using $NH_3 + NH_4^+$ as the total NH_3 but only NO_3^- as the total HNO_3; Simulation 2) and (d–f) the Simulation 2 and the simulation with both estimated gas-phase NH_3 and HNO_3 information (this study; Simulation 3). Filled circles in light blue, light green, light yellow, and light red colors represent daily data belong to the *local ventilation with no regional transport* (V-nT) group, *local stagnation with no regional transport* (S-nT) group, *local ventilation with regional transport* (V-T) group, and *local stagnation with regional transport* (S-T) group, respectively. Gray solid lines indicate a 1-to-1 relationship.

2. The reconstructed concentrations certainly introduce uncertainty, which the authors recognize. For example, they comment (lines 122-123): “Although there are uncertainties in the reconstructed NH_3 and HNO_3 due to lack of direct measurements, their impact on the estimation of inorganic ALW and particle pH may be small enough.” They follow this comment by a discussion on why the impact may be small enough. In my opinion, there is too much uncertainty here (in the data and the language, e.g. “may” and “would”), and I suggest that the authors conduct a sensitivity analysis on how uncertainty in the reconstructed concentrations of NH_3 and HNO_3 affects their conclusions.

As the reviewer suggested, we conducted sensitivity tests to examine how various NH_3 levels can affect and change the results, particularly pH and inorganic partitioning ratios [$\varepsilon(NO_3^-)$ and $\varepsilon(NH_4^+)$]. Various NH_3 levels from 0 ppb to 50 ppb are applied for all the measurement days as fixed values (no day-to-day variations in NH_3).

In the reconstructed NH_3 data contains two types of error that are (i) from the day-to-day estimation by the multiple regression model (Text S1 and Table S1) and (ii) from the average concentration of NH_3 in Seoul. Figs. 5a, c, and e show good correlations between the results from simulation with daily varied NH_3 (average of 10.9 ppb) and that with daily fixed NH_3 [e.g., R^2 values of 0.779 for pH, 0.984 for $\varepsilon(NO_3^-)$, and 0.575 for $\varepsilon(NH_4^+)$ in 10 ppb]. If the fixed NH_3 level was not 0 ppb, correlations with 5, 10, 20, and 40 ppb are not significantly different. Therefore, the potential errors in pH and partitioning ratios raised from the day-to-day estimation seem to be limited. Figs. 5b, d, and f show that the average pH and partitioning ratios for each categorized group become flattened over the 5 ppb of NH_3. This can be already expected from the buffering effect of NH_3–NH_4^+

partitioning on pH, and thus the potential errors from the estimation of NH$_3$ do not change our conclusion.

Based on the sensitivity test, we removed words representing uncertainty from this section, and we added the content related to the sensitivity test for NH$_3$ to Line 130 on page 5 of the original manuscript as follows:

We conducted ISORROPIA simulations with various NH$_3$ levels (0–50 ppb) applied for all the measurement days as fixed values to further explore the sensitivity of pH, $\varepsilon(\mathrm{NO_3^-})$, and $\varepsilon(\mathrm{NH_4^+})$ to NH$_3$. Good correlations between results from the daily varied NH$_3$-simulation and the fixed NH$_3$-simulations shows that potential errors induced by the estimation of daily NH$_3$ levels will be small if NH$_3$ concentrations are nonzero (Figs. 5a, c, and e). Increasing pH and $\varepsilon(\mathrm{NO_3^-})$ and decreasing $\varepsilon(\mathrm{NH_4^+})$ by the increase in fixed NH$_3$ level become flatten over the range from a half to 2 times of the average NH$_3$ concentration in Seoul (~5–20 ppb; Phan et al., 2013) (Figs. 5b, d, and f), and this indicates that the potential errors in reconstructed NH$_3$ will not significantly change the results in this study.

Also, we added Fig. 5 into the manuscript in the revised version.

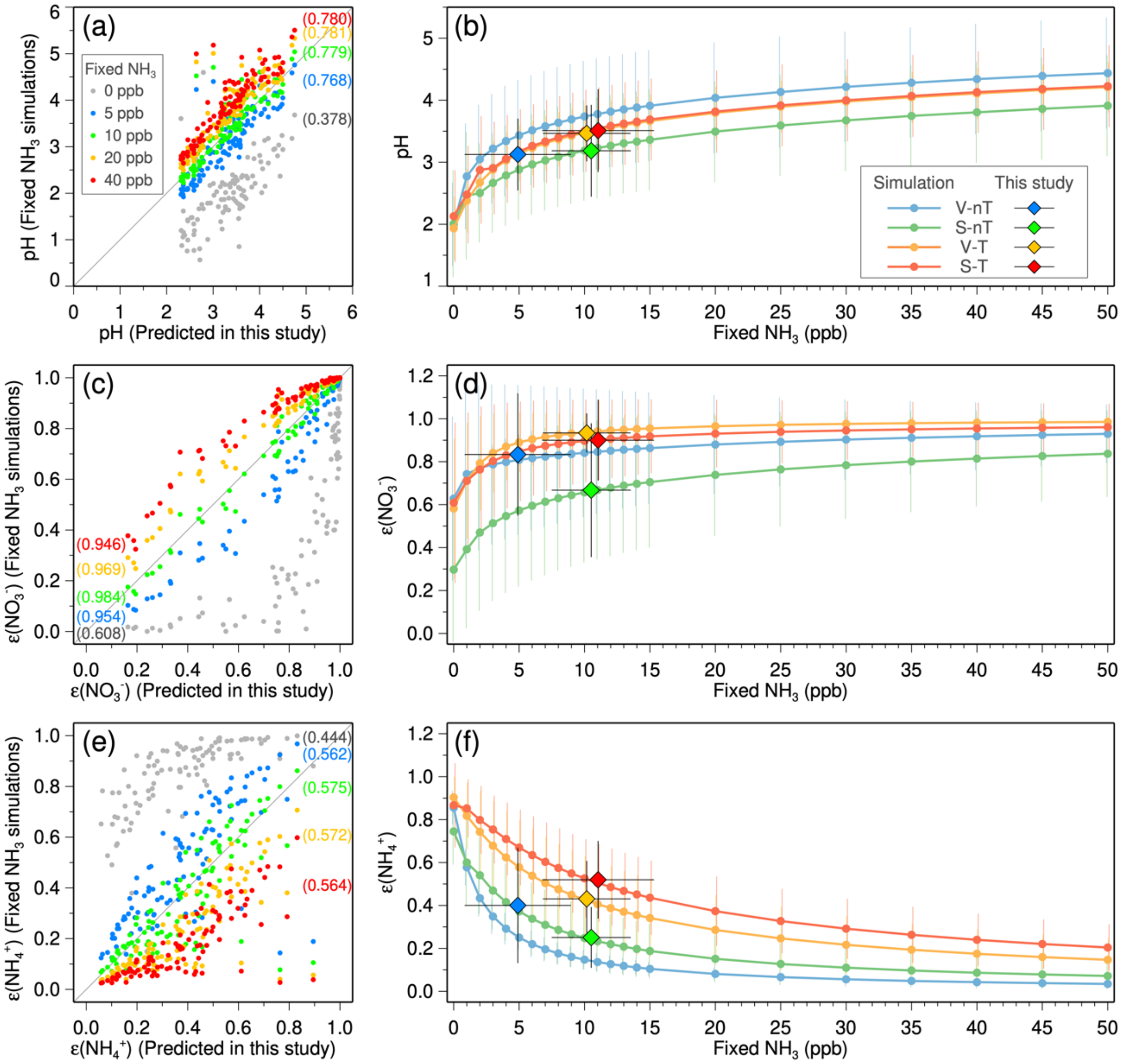

Figure 5: Sensitivity of (a–b) predicted pH, (c–d) nitrate partitioning ratio [$\varepsilon(\mathrm{NO_3^-}) = \mathrm{NO_3^-} / (\mathrm{HNO_3} + \mathrm{NO_3^-})$], and (e–f) ammonium partitioning ratio [$\varepsilon(\mathrm{NH_4^+}) = \mathrm{NH_4^+} / (\mathrm{NH_3} + \mathrm{NH_4^+})$] to gas-phase ammonia (NH$_3$) concentrations. (a, c, and e) Comparisons between the simulation in this study (using the daily reconstructed NH$_3$ concentrations) and the simulations with the various fixed NH$_3$ levels (colored dots in gray, blue, green, yellow, and red for 0 ppb, 5 ppb, 10 ppb, 20 ppb, and 40 ppb, respectively). Values in round brackets are the R-squared values of the linear regressions. Gray solid lines indicate a 1-to-1 relationship. (b, d, and f) Average (solid circles) and standard deviation (vertical bars) of pH, $\varepsilon(\mathrm{NO_3^-})$, and $\varepsilon(\mathrm{NH_4^+})$ for the *local ventilation with no regional transport* (V-nT) group (light blue), *local stagnation with no regional transport* (S-nT) group (light green), *local ventilation with regional transport* (V-T) group (light yellow), and *local stagnation with regional transport* (S-T) group (light red) with respect to the various fixed NH$_3$ levels from 0 ppb to 50 ppb.

Averages and standard deviations of the reconstructed NH_3 concentrations and obtained pH, $\varepsilon(NO_3^-)$, and $\varepsilon(NH_4^+)$ for the V-nT, S-nT, V-T, and S-T groups are represented as blue, green, yellow, and red diamonds with horizontal and vertical bars.

Minor and technical comments:

Line 12: replace ‘stagnant’ with ‘stagnation’

Thanks for the correction. It was now corrected.

Line 17: replace ‘group’ with ‘grouped’ or otherwise revise as this is unclear

We revised the sentence as follows:

$PM_{2.5}$ measured under the condition of regional transport from the upwind source areas in China was higher in mass concentration and richer in secondary inorganic aerosol (SIA) species and aerosol liquid water (ALW) compared to that measured under the non-transport condition.

Lines 32-35: the sentence is unclear, especially the second half (. . . “ and also a situation. . .”). Please revise (splitting into two sentences would probably help).

As the reviewer suggested, we split the sentence into two as follows:

Synoptic weather conditions cause stagnation and long-range transport that can lead to the accumulation of particles and gaseous precursors from local and remote sources. It can also change local meteorological factors to favorable conditions for secondary aerosol production, such as photo-oxidation and aqueous-phase processing (Sun et al., 2014; Zheng et al., 2015; Seo et al., 2017).

Line 86: “The OM identified in this study is ～5% of the total OM.” I think I know what you mean, but this sentence is confusing to me. Perhaps rephrase as “The organic compounds identified in this study constitute ～5% of the total OM.”

The sentence was now revised as suggested by the reviewer.

Line 255: replace ‘the more increase’ with ‘the higher increase’?

‘the more increase’ is now replaced with ‘the higher increase.’

Lines 291-292: “Interestingly, SOR increase by temperature (and also irradiance) is not significant as much as inorganic ALW (Figs. 8c) despite. . .” please revise this phrase as it is not clear.

We revise the sentence as follows:

Interestingly, the increasing SOR by temperature (and also irradiance) is not significant as much as that by inorganic ALW (Figs. 8c) despite the high-temperature and strong-irradiance conditions conducive to photochemical oxidation of SO_2 in summer.

Lines 293-295: “This implies that the observed high SO_4 in the S-T group was induced by the aqueous-phase oxidation of SO_2 in the transported wet particles rather than the photochemical gas-phase oxidation.” It seems appropriate to point out here that gas-phase oxidation likely also played a role (i.e. the data do not rule out gas-phase oxidation as a source of sulfate).

As the reviewer suggested, we modified the sentence not to rule out gas-phase oxidation as follows:

This implies that the observed high SO_4^{2-} in the S-T group resulted not only from the photochemical gas-phase oxidation but also considerably from the aqueous-phase oxidation of SO_2 in the transported wet particles.

There are several instances where the article “the” is overused. As an example, last sentence in the abstract: “This study reveals the synergistic effect of remote and local sources on the urban haze pollution in the downwind region and provides insight into the nonlinearity of domestic and foreign contributions to receptor

$PM_{2.5}$ concentrations in the numerical air quality models”. I would suggest removing “the” in front of ‘urban’, ‘numerical air quality models’. This seems more consistent with common usage and would also further help to suggest applicability of the conclusions to other areas. I suggest the authors review the whole manuscript for use of “the”.

Thank you for comments. We removed several “the” in the revised version of manuscript following the reviewer’s suggestion.

Synergistic enhancement of urban haze by nitrate uptake into transported hygroscopic particles in the Asian continental outflow

Jihoon Seo[1,2], Yong Bin Lim[3], Daeok Youn[4], Jin Young Kim[1], Hyoun Cher Jin[1]

[1]Environment, Health and Welfare Research Center, Korea Institute of Science and Technology, Seoul, 02792, South Korea
[2]School of Earth and Environmental Sciences, Seoul National University, Seoul, 08826, South Korea
[3]Departmant of Chemical Engineering and Material Science, Ewha Womans University, Seoul, 03760, South Korea
[4]Departmant of Earth Science Education, Chungbuk National University, Cheongju, 28644, South Korea

Correspondence to: Jin Young Kim (jykim@kist.re.kr)

Abstract. Haze pollution is affected by local air pollutants, regional transport of background particles and precursors, atmospheric chemistry related to secondary aerosol formation, and meteorological conditions conducive to the physical, dynamical, and chemical processes. In the large, populated and industrialized areas like the Asian continental outflow region, the combination of regional transport and local stagnation often exacerbates urban haze pollution. However, the detailed chemical processes underlying the enhancement of urban haze induced by the combined effect of local emissions and transported remote pollutants are still unclear. Here, we demonstrate an important role of transported hygroscopic particles in increasing local inorganic aerosols, by studying the chemical composition of $PM_{2.5}$ collected between October 2012 and June 2014 in Seoul, a South Korean megacity in the Asian continental outflow region, using the ISORROPIA II thermodynamic model. $PM_{2.5}$ measured under the condition of regional transport from the upwind source areas in China was higher in mass concentration and richer in secondary inorganic aerosol (SIA) species (SO_4^{2-}, NO_3^-, and NH_4^+) and aerosol liquid water (ALW) compared to that measured under the non-transport condition. The secondary inorganic species and ALW were both increased, particularly in cases with high $PM_{2.5}$ levels, and this indicates inorganic species as a major driver of hygroscopicity. We conclude that the urban haze pollution in the continental outflow region like Seoul, particularly during the cold season, can be exacerbated by ALW in the transported particles, which enhances the nitrate partitioning into the particle phase in NO_x- and NH_3-rich urban areas. This study reveals the synergistic effect of remote and local sources on urban haze pollution in the downwind region and provides insight into the nonlinearity of domestic and foreign contributions to receptor $PM_{2.5}$ concentrations in numerical air quality models.

삭제됨: stagnant

삭제됨: Measured

삭제됨: group

삭제됨: SIA

삭제됨: the

삭제됨: the

1 Introduction

Fine particulate matter (under 2.5 µm in diameter; $PM_{2.5}$) in urban areas consists of inorganic species (SO_4^{2-}, NO_3^-, and NH_4^+) and organic matter (OM) produced by the gas-to-particle conversion of anthropogenic and biogenic precursors (Seinfeld and Pandis, 2016). These particles pose a public health problem due to their adverse effects on the human respiratory and cardiovascular systems (Pope and Dockery, 2006). Consequently, many countries have tried to mitigate urban haze pollution by reducing local precursor emissions (van der A et al., 2017; Kim and Lee, 2018). However, since air pollution is also influenced by transported air pollutants, it is difficult to achieve improved air quality in megacities located in large, populated, and industrialized areas by controlling local emissions (Seo et al., 2018). Synoptic weather conditions cause stagnation and long-range transport that can lead to the accumulation of particles and gaseous precursors from local and remote sources. It can also change local meteorological factors to favorable conditions for secondary aerosol production, such as photo-oxidation and aqueous-phase processing (Sun et al., 2014; Zheng et al., 2015; Seo et al., 2017). Therefore, a better understanding of the combined effects of local emissions, regional transport, and meteorological conditions on urban haze pollution is required to establish appropriate mitigation strategies.

삭제됨: and

삭제됨: a situation that is exacerbated by

삭제됨: conducive

One key aerosol component that affects the formation and growth of haze particles is aerosol liquid water (ALW), which is ubiquitous and abundant in tropospheric fine particles (Nguyen et al., 2016). ALW not only increases the mass of secondary organic aerosols (SOA) by facilitating the partitioning of gas-phase water-soluble OM into the condensed phase, followed by aqueous-phase reactions (Asa-Awuku et al., 2010; Carlton and Turpin, 2013; McNeill, 2015; Marais et al., 2016), but also enhances the secondary inorganic aerosol (SIA) mass via nitrate formation through HNO_3 uptake and N_2O_5 hydrolysis (Zhang et al., 2015; Wang et al., 2017), and via sulfate production through the aqueous oxidation of SO_2 (Cheng et al., 2016; Wang et al., 2017). Studies of urban haze in the North China Plain reported simultaneous elevation of the relative humidity (RH), ALW, and SIA, which indicates the hygroscopic properties of inorganic species and the role of ALW in mass transfer into the particles (Liu et al., 2017; Tie et al., 2017; Wu et al., 2018). Combined with the ambient temperature and particle pH, ALW is critical for gas–particle partitioning of inorganic and water-soluble organic acid gases (Guo et al., 2018; Nah et al., 2018). Therefore, regional transport of wet particles to the precursor-rich urban environment will affect haze pollution downwind.

삭제됨: (NCP)

삭제됨: SIA

The South Korean capital city of Seoul and its metropolitan area is one of the highly populated megacities in East Asia, with a population of 25 million people, 9 million vehicles, and nearly half of the national gross domestic product, and has suffered from episodic haze events, particularly during the cold season (Seo et al., 2017; 2018). Although the Seoul metropolitan area is a large anthropogenic emission source of nitrogen oxides (NO_x), ammonia (NH_3), and volatile organic compounds (VOCs) (NIER, 2018), the effect of transported air pollutants from China cannot be ignored because of its location downwind from the major emission source region in China like the North China Plain and Yangtze River Delta (Fig. S1). In particular, severe multiday haze events in the Seoul metropolitan area mostly occur with a specific synoptic pattern, such as an eastward-moving high-pressure system, which induces regional transport of air pollutants from China and, subsequently, local stagnation (Seo et al., 2017; 2018). Therefore, the haze pollution in Seoul becomes severe primarily by accumulation of local and transported air pollutants. However, a recent numerical modeling study on regional contribution to the particulate concentration in Seoul reported a discrepancy between responses to the reduction of domestic and foreign emissions (Kim et al., 2017), and this implies additional production and growth of local haze particles by nonlinear interactions between local emissions and transported pollutants.

삭제됨: (GDP),

삭제됨: Metropolitan Area (SMA)

삭제됨: NCP

삭제됨: YRD) (

삭제됨: SMA

In this study, we explore the combined effects of local and remote sources, ALW and particle pH, and meteorological factors on the formation and growth of urban haze particles, based on daily measurement of $PM_{2.5}$ chemical compositions in Seoul, backward trajectory analysis, and the ISORROPIA II thermodynamic model (Fountoukis and Nenes, 2007). Different chemical compositions and characteristics of Seoul haze according to the regional transport from China and the local stagnation in the Seoul metropolitan area is investigated from the perspective of inorganic partitioning and water uptake processes. An effective strategy for $PM_{2.5}$ reduction in Seoul is further discussed using ambient NO_x and NH_3 levels, and analytic calculation of the HNO_3–NO_3^- partitioning ratio as a function of ALW, pH, and temperature.

삭제됨: the NCP and YRD areas

삭제됨: SMA

삭제됨: nitrate

2 Data and methods

2.1 Measurements and chemical analysis

Daily $PM_{2.5}$ sampling was conducted on 210 days between October 2012 and June 2014 at the Korea Institute of Science and Technology (KIST) site in northeastern Seoul (37.603°N, 127.047°E, 58 m above sea level; Fig. S1). $PM_{2.5}$ samples for determining inorganic and carbonaceous species were collected on 47-mm Teflon filters (Pall Corporation, Port Washington, NY, USA) with a Teflon-coated aluminum cyclone (URG Corporation, Chapel Hill, NC, USA) at a flow rate of 16.7 L/min, and on 203 × 254-mm quartz fiber filters (Whatman, Maidstone, UK) with a high-volume air sampler (flow rate of 1,000 L/min; Andersen Instruments, Atlanta, GA, USA), respectively.

The concentrations of inorganic ions (SO_4^{2-}, NO_3^-, Cl^-, NH_4^+, K^+, Ca^{2+}, Na^+, and Mg^{2+}) were measured using a 2000i/SP ion chromatograph (Dionex, Sunnyvale, CA, USA) after sonicating the Teflon filter sample for 30 min in a mixture of 0.5 mL of ethanol and 14.5 mL of distilled deionized water. Using a piece of the quartz fiber filter sample (10 × 15 mm), the concentrations of organic carbon (OC) and elemental carbon (EC) were measured using a thermal/optical carbon aerosol analyzer (Sunset Laboratory, Tigard, OR, USA) based on National Institute for Occupational Safety and Health (NIOSH) method 5040 (Birch and Cary, 1996). We also identified 17 *n*-alkanes (C_{20}–C_{36}), 15 polycyclic aromatic hydrocarbons (PAHs; C_{14}–C_{24}), 19 monocarboxylic acids (C_6–C_{20}), 19 dicarboxylic acids (C_3–C_{11}), and 10 sugars (C_5–C_6, and C_{12}) using the extract from one-half of the quartz fiber filter sample and a 7890A gas chromatograph (Hewlett Packard, Palo Alto, CA, USA) coupled to a 5975C mass selective detector (Agilent, Santa Clara, CA, USA). The OM / OC ratios derived from the measured OM and OC concentrations were used to estimate the total OM concentration. The organic compounds identified in this study constitute ~5% of the total OM. The analytical procedures used herein are described in detail elsewhere (Seo et al., 2017; Kim et al., 2018). In this study, out of 210 sampling days, 118 daily data that include not only inorganic species but also OM based on the identified organic compounds' information were selected and utilized (Fig. S2).

삭제됨: OM

삭제됨: is

Note that the $PM_{2.5}$ sampling on Teflon filter for inorganic ions was conducted without both a denuder and backup filters, and thus there could be potential sampling artifacts on the results, particularly negative artifacts in semivolatile ammonium nitrate (Ashbaugh and Eldred, 2004; Chow et al., 2005). Nie et al. (2010) reported that summertime nitrate loss on Teflon filter from the un-denuded filter sampling without backup filters is to be ~75% at lower nitrate concentrations (< 10 μg m^{-3}) but only ~10% at higher nitrate concentrations (> 10 μg m^{-3}) due to the formation of particle cake. Considering small evaporative loss in the cold season and the high nitrate concentration in Seoul, we expected small to moderate sampling errors in this study.

Sensitivity tests considering potential ammonium nitrate loss from the filter samples show that the assumption of 20% nitrate loss for the high concentrations with low-temperature groups and 50% nitrate loss for the low concentrations with moderate temperature group does not change our conclusion (Fig. S8).

The hourly concentrations of SO_2, NO_2, CO, O_3, and PM_{10} at 34 air quality monitoring sites in Seoul (Fig. S1) provided by the Korea Ministry of Environment (KMOE) were averaged over all sites for each day, to obtain representative daily concentrations of each species for Seoul (Korea Environment Corporation, 2019). The hourly meteorological data of temperature, RH, wind speed, and solar irradiance at the Seoul weather station (37.571°N, 126.966°E) managed by the Korea Meteorological Administration (KMA) were averaged for each day and used in our analysis (KMA, 2019). Boundary layer height (BLH) were derived from the European Centre for Medium-Range Weather Forecasts Reanalysis Interim (ERA-Interim) data (Dee et al., 2011; http://apps.ecmwf.int/datasets/data/interim-full-daily/, last access: 23 October 2019) at a grid point in Seoul (37.5°N, 127.0°E).

2.2 Categorization of measurements

To categorize the daily measurements according to (1) local atmospheric conditions (stagnation or ventilation) and (2) regional impact (transport of pollutants from upwind source area), we used the 72-h backward trajectories from 500 m above the sampling site, obtained with the Hybrid Single-Particle Lagrangian Integrated Trajectory (HYSPLIT) model (https://ready.arl.noaa.gov; Stein et al., 2015) for every hour of each measurement day. We defined a local source area (Seoul metropolitan area) and two major upwind source areas in China (North China Plain and Yangtze River Delta) based on the satellite tropospheric NO_2 column density distribution (Fig. 1a), and calculated average residence time of daily 24 trajectories in the Seoul metropolitan area (t_{SMA}) and the two source areas in China (t_{CHN}). The daily average residence time in each area shows different source characteristics such as the smaller sulfur-to-nitrogen emission ratio in Seoul (~0.06; 4.5 kt of SO_x and 71.1 kt of NO_x in 2010; NIER, 2018) compared with that of the Jing-Jin-Ji region in the North China Plain (~0.71; 2010 kt of SO_2 and 2830 kt of NO_x in 2010; Li et al., 2017). For example, t_{CHN} is highly correlated not only with particulate SO_4^{2-} and NO_3^- concentrations but also with their precursors (SO_2 and NO_2) concentrations, while t_{SMA} has statistically significant correlation only with NO_2 concentration (Fig. S3).

Since the medians of both t_{SMA} and t_{CHN} (for $t_{CHN} \neq 0$ h days) were ~6 h, we applied the 6 h as a reference trajectory residence time to categorize daily measurement data into relatively stronger and weaker influences by the local stagnation in the Seoul metropolitan area (with t_{SMA}) and the regional transport from China (with t_{CHN}). The measurement days were classified into one of four groups and summarized in Table 1: (i) the *local ventilation with no regional transport* (V-nT), in which the trajectories did not originate from the source areas in China and also were not stagnant in the Seoul metropolitan area ($t_{SMA} <$ 6 h and $t_{CHN} = 0$ h; $n = 9$ days), (ii) the *local stagnation with no regional transport* (S-nT), in which the trajectories did not originate from the source areas in China but were stagnant in the Seoul metropolitan area ($t_{SMA} \geq 6$ h and $t_{CHN} = 0$ h; $n = 15$ days), (iii) the *local ventilation with regional transport* from the Chinese source area (V-T), in which the trajectories originated from the source areas in China but were not stagnant in the Seoul metropolitan area ($t_{SMA} < 6$ h and $t_{CHN} \geq 6$ h; $n = 15$ days),

삭제됨: 2.2

[1] 이동함(삽입)

[2] 이동함(삽입)

[3] 이동함(삽입)

and (iv) the *local stagnation with regional transport* from the Chinese source area (S-T), in which the trajectories originated from the source areas in China and also were stagnant in the Seoul metropolitan area ($t_{SMA} \geq 6$ h and $t_{CHN} \geq 6$ h; $n = 21$ days). The trajectory density distribution in the North China Plain and Yangtze River Delta areas were characterized for each group, with few trajectories for the *no regional transport* (V-nT and S-nT) groups but relatively dense trajectories for the *regional transport* (V-T and S-T) groups (Fig. 1b–d).

[4] 이동함(삽입)

Despite the various potential factors like emissions, atmospheric chemistry, and meteorology that can affect the gas and particulate air quality, the simple categorization according to the residence time of backward trajectories could reveal different characteristics in chemical species and meteorological factors associated with the local stagnation and the regional transport of air pollutants. For example, the average concentrations of primary gaseous pollutants (SO_2, NO_2, and CO) of the *local stagnation with regional transport* (S-T) group are significantly higher than those of the *local stagnation with no regional transport* (S-nT) group ($p \leq 0.001$), although average local meteorological factors between the two groups do not show significant differences (Table 2 and Figs. 2 and 3). On the other hand, the lower wind speed and shallower BLH were seen in the *local stagnation* (S-T and S-nT) groups compared with the *local ventilation* (V-T and V-nT) groups (Fig. 2), and the *local stagnation with regional transport* (S-T) group shows significantly higher levels of SO_2, NO_2, and CO in comparison with the *local ventilation with regional transport* (V-T) group, probably related to accumulation in the stagnant condition. Note that although the present study used a part of total daily data that OM concentrations are available ($n = 118$), composite averages and differences of meteorological variables and air pollutant concentrations among the four categorized groups using the total daily data including the OM-unavailable dates ($n = 210$) showed the same characteristics as shown in Figs. 2 and 3 (Fig. S4).

2.3 Prediction of ALW content and pH

ISORROPIA II thermodynamic model was run in forward mode to estimate ALW content associated with inorganic species, pH, and the equilibrium gas–particle partitioning based on the daily $PM_{2.5}$ ionic compositions, RH, and temperature. ISORROPIA II uses total (gas- plus aerosol-phase) measurements as inputs, under the metastable assumption (no solid precipitates). Recent validation studies demonstrate that forward mode is influenced less by measurement errors and gives a more accurate pH than reverse mode, which uses only the aerosol-phase composition as an input (Hennigan et al., 2015; Song et al., 2018).

The forward mode of ISORROPIA II requires the total NH_3 (gas-phase NH_3 plus particulate NH_4^+), total HNO_3 (HNO_3 plus particulate NO_3^-), and total Cl (gas-phase HCl plus particulate Cl^-) concentrations, as well as the particulate SO_4^{2-}, K^+, Ca^{2+}, Na^+, and Mg^{2+} concentrations. However, the ambient NH_3, HNO_3, and HCl data were not available for this study. To overcome this problem with the input data, we used statistically reconstructed NH_3 data and then estimated HNO_3 using a thermodynamic model.

삭제됨:

Firstly, the daily NH_3 concentrations in Seoul from January 2012 to December 2014 were reconstructed using the statistical characteristics of a year-long record of NH_3 at the Gwangjin site (37.545°N, 127.096°E) in Seoul for the preceding year (346 days between September 2010 and August 2011; Phan et al., 2013). There were small interannual changes in the estimated

NH_3 emission in Seoul (Fig. S5; NIER, 2018), and both two sites share similar environments located downwind from the downtown core under the prevailing westerlies and surrounded by residential and small urban green areas (Fig. S1). Therefore, we assumed that the statistical characteristics of both two sites and periods would be similar despite the temporal gap (~1–3 yr) and spatial distance (~7.8 km) between this study and Phan et al. (2013). We built a multiple linear regression model of NH_3 that retains statistical characteristics of the measured NH_3 such as the annual average and standard deviation of 10.9 ± 4.25 ppb and the significant linear correlations ($p < 0.05$) with temperature, RH, wind speed, and SO_2, NO_2, and CO concentrations (Text S1 and Table S1). The reconstructed NH_3 concentration is seasonally high during the warm season as reported by Phan et al. (2013) and shows high peaks on the polluted days with stagnant condition in the cold season (Fig. S6). In the next step, the ISORROPIA II calculation was performed, using the reconstructed NH_3 and measured NH_4^+ as the total equivalent NH_3, and the measured NO_3^- alone as the total HNO_3, to estimate the HNO_3–NO_3^- partitioning ratio. Then, using both the measured NO_3^- and the ratio between the HNO_3 and NO_3^- predicted from the initial result, we estimated the ambient HNO_3. Note that we regarded the HNO_3 / NO_3^- ratio as approximately independent of the total HNO_3. Although the nitrate partitioning depends on temperature, ALW content, and pH in general, the HNO_3 / NO_3^- ratio is affected alone by pH because both temperature and ALW are independent variables in this step. In the existence of excess NH_3 as we assumed for Seoul (~10 ppb at the first step), changes in pH by total HNO_3 are limited owing to the buffering effect of NH_3–NH_4^+ partitioning (Weber et al., 2016; Guo et al., 2018; Lim et al., 2020). The pH, nitrate partitioning ratio [$\varepsilon(NO_3^-) = NO_3^- / (HNO_3 + NO_3^-)$], and ammonium partitioning ratio [$\varepsilon(NH_4^+) = NH_4^+ / (NH_3 + NH_4^+)$] from the ISORROPIA simulations with and without gas-phase HNO_3 information show negligible differences between each other (Figs. 4d–f), unlike the significant role of additional NH_3 information on increasing pH and $\varepsilon(NO_3^-)$ and decreasing $\varepsilon(NH_4^+)$ (Figs. 4a–c). Finally, we repeated the ISORROPIA simulation with both total NH_3 and total HNO_3 estimated from the previous steps. Here we did not consider HCl–Cl^- partitioning because the Cl^- fraction in dry $PM_{2.5}$ (~1% in average) is significantly smaller than the NO_3^- and NH_4^+ fractions (~18% and ~12% in average, respectively).

Although there are uncertainties in the reconstructed NH_3 and HNO_3 due to lack of direct measurements, their impact on the estimation of inorganic ALW and particle pH is small enough. The good agreement between the predicted and statistically reconstructed NH_3 concentrations ($R^2 \sim 0.95$), as well as between the predicted and measured SO_4^{2-}, NO_3^-, and NH_4^+ concentrations ($R^2 > 0.95$; Fig. S7), ensures small errors on water contents of individual inorganic species. Since water uptake by inorganic aerosol in the ISORROPIA II is based on the Zdanovskii-Stokes-Robinson (ZSR) mixing rule (Stokes and Robinson, 1966), which approximates the water content of a mixture as a sum of water contents of individual salts at the same RH (Fountoukis and Nenes, 2007), expected error in W_i induced by potential errors in NH_3 and HNO_3 would also be small. Regarding pH, buffering effect of semivolatile NH_3 partitioning reduces sensitivity of pH to excess NH_3 in the NH_3-rich conditions like Seoul (Weber et al., 2016; Guo et al., 2018; Lim et al., 2020). We conducted ISORROPIA simulations with various NH_3 levels (0–50 ppb) applied for all the measurement days as fixed values to further explore the sensitivity of pH, $\varepsilon(NO_3^-)$, and $\varepsilon(NH_4^+)$ to NH_3. Good correlations between results from the daily varied NH_3-simulation and the fixed NH_3-simulations shows that potential errors induced by the estimation of daily NH_3 levels will be small if NH_3 concentrations are

[5] 이동함(삽입)

삭제됨: S3).

삭제됨: may be

삭제됨: S4

삭제됨: may reduce sensitivity of pH to excess NH_3 in the NH_3-rich conditions like Seoul (Weber et al., 2016).

nonzero (Figs. 5a, c, and e). Increasing pH and $\varepsilon(NO_3^-)$ and decreasing $\varepsilon(NH_4^+)$ by the increase in fixed NH_3 level become flatten over the 5 ppb of NH_3 (Figs. 5b, d, and f), and this indicates that the potential errors in reconstructed NH_3 will not significantly change the results in this study.

Since ALW content associated with OM (W_o) is not considered in the ISORROPIA II, we estimated it according to the κ-Köhler theory and the ZSR mixing rule (Nguyen et al., 2015, and references therein) by the following equation:

$$W_o = V_o \kappa_{org} \frac{a_w}{1-a_w} \quad (1)$$

where V_o is volume of OM (μm^3 cm^{-3}), which is obtained from OM concentration (μg m^{-3}) divided by a typical organic density of 1.4 g cm^{-3} (Turpin and Lim, 2001), κ_{org} is hygroscopicity parameter (dimensionless) calculated from the parameterized relationship of $\kappa_{org} = (0.29 \pm 0.05) \cdot (O/C)$ for the range of O / C from 0.3 to 0.6 (Chang et al., 2010), and a_w is water activity (dimensionless) that is assumed to be equivalent to RH (Nguyen et al., 2016).

3 Results and discussion

3.1 Effects of regional transport and local stagnation on $PM_{2.5}$ composition

Average concentrations of $PM_{2.5}$ and chemical components were highest in the *local stagnation with regional transport* (S-T) group (e.g., $PM_{2.5\ dry}$ of 72.2 μg m^{-3}) and lowest in the *local ventilation with no regional transport* (V-nT) group (e.g., $PM_{2.5\ dry}$ of 19.9 μg m^{-3}), and the average concentrations for the *local ventilation with regional transport* (V-T) group and the *local stagnation with no regional transport* (S-nT) groups (e.g., $PM_{2.5\ dry}$ of 53.3 μg m^{-3} and 34.4 μg m^{-3}, respectively) located between that of the S-T and V-nT groups (Table 2 and Fig. 3f). The composite difference between the *regional transport* (V-T and S-T) groups and *no regional transport* (V-nT and S-nT) groups reveals the regional effect of transported haze particles and precursors from the North China Plain and Yangtze River Delta, while that between the *local stagnation* (S-T and S-nT) groups and *local ventilation* (V-T and V-nT) groups shows the effect of accumulation or diffusion of both local and transported pollutants in the Seoul metropolitan area. Thus, the significant difference of each $PM_{2.5}$ component between the S-T and V-nT groups (Fig. 6) indicates both contributions of local stagnant condition over the Seoul metropolitan area and regional transport from the Chinese source area to the exacerbation of haze pollution in Seoul.

The average concentrations of gaseous precursors like SO_2 and NO_2 for the S-T group were about 2 times higher than those for the V-nT group (Fig. 3), while SO_4^{2-}, NO_3^-, and NH_4^+, and inorganic ALW increased by 5–10 times (Fig. 6). In contrast, average OM concentration for the S-T group was 2 times higher than that for the V-nT group similarly to CO, and organic ALW of the S-T group showed a relatively smaller increase (~4 times of the V-nT group) than inorganic ALW (~8 times of the V-nT group). Therefore, the $PM_{2.5}$ increase in Seoul seems to be induced not only by the physical and dynamical processes like transport or accumulation of air pollutants but also by the chemical process like secondary aerosol formation, particularly related to the increase in inorganic species and ALW.

[1] 위로 이동함: Categorization of measurements
To categorize the daily measurements according to (1) local atmospheric conditions (stagnation or ventilation) and (2) regional impact (transport of pollutants from upwind source area), we used the 72-h backward trajectories from 500 m above the sampling site, obtained with the Hybrid Single-Particle Lagrangian Integrated Trajectory (HYSPLIT) model (https://ready.arl.noaa.gov; Stein et al., 2015) for every hour of each measurement day.

삭제됨: 2.3

[2] 위로 이동함: (~0.71; 2010 kt of SO_2 and 2830 kt of NO_x in 2010; Li et al., 2017). For example,

[3] 위로 이동함: For example, t_{CHN} is highly correlated not only with particulate SO_4^{2-} and NO_3^- concentrations but also with their precursors (SO_2 and NO_2) concentrations, while t_{SMA} has statistically significant correlation only with NO_2 concentration (Fig.

[5] 위로 이동함: S6).

삭제됨: We defined a local source area (SMA) and two major upwind source areas in China (NCP and YRD) based on the satellite tropospheric NO_2 column density distribution (Fig. 1a), and calculated average residence time of daily 24 trajectories in the SMA area (t_{SMA}) and the NCP and YRD areas in China (t_{CHN}). The daily average residence time in each area shows different source characteristics such as the smaller sulfur-to-nitrogen emission ratio in Seoul (~0.06; 4.5 kt of SO_x and 71.1 kt of NO_x in 2010; NIER, 2018) compared with that of the Jing-Jin-Ji region in the NCP

삭제됨: S5).
Since the medians of both t_{SMA} and t_{CHN} (for $t_{CHN} \neq 0$ h days) were ~6 h, we applied the 6 h as a reference trajectory residence time to categorize daily measurement data into relatively stronger and weaker influences by the local stagnation in the SMA (with t_{SMA}) and the regional transport from the NCP and YRD (with t_{CHN}). The measurement days were classified into one of four groups and summarized in Table 1: (i) the *local ventilation with no regional transport* (V-nT), in which the trajectories did not originate from the NCP and YRD and also were not stagnant in the SMA ($t_{SMA} < 6$ h and $t_{CHN} = 0$ h; $n = 9$ days), (ii) the *local stagnation with no regional transport* (S-nT), in which the trajectories did not originate from the NCP and YRD but were stagnant in the SMA ($t_{SMA} \geq 6$ h and $t_{CHN} = 0$ h; $n = 15$ days), (iii) the *local ventilation with regional transport* from the Chinese source area (V-T), in which the trajectories originated from the NCP and YRD but were not stagnant in the SMA ($t_{SMA} < 6$ h and $t_{CHN} \geq 6$ h; $n = 15$ days), and (iv) the *local stagnati* ...

[4] 위로 이동함: areas were characterized for each group, with few trajectories for the *no regional transport* (V-nT and S-nT) groups but

삭제됨: NCP and YRD

삭제됨: SMA.

삭제됨: 4

삭제됨: SMA

삭제됨: SIA species

삭제됨: the

삭제됨: 4

삭제됨: SIA

삭제됨: inorganic

Statistically significant difference ($p < 0.05$) between the S-T and S-nT groups (effect of regional transport in the local stagnant condition) was observed in SIA species (SO_4^{2-}, NO_3^-, and NH_4^+), OM, and ALW (both W_i and W_o), and that between the S-T and V-T groups (effect of local stagnation in the regional transport condition) was seen for EC and OM (Table 2). Thus, although both regional transport and local stagnation can induce high concentrations of $PM_{2.5}$ and its chemical components of the S-T group, the effect of regional transport is more significant for the increase in inorganic species and water content, while the effect of local stagnation is more significant for the increase in carbonaceous species. Sulfur oxidation ratio [SOR = SO_4^{2-} / (SO_2 + SO_4^{2-})], nitrate partitioning ratio [$\varepsilon(NO_3^-)$], and ammonium partitioning ratio [$\varepsilon(NH_4^+)$] of the S-T group, which were significantly higher than that of the S-nT group ($p < 0.05$) but did not clearly differ from that of the V-T group, indicate that the increase in SIA by the regional transport effect is closely associated with the enhanced oxidation (e.g., from NO_x to HNO_3) or partitioning of inorganic species into the particle phase.

삭제됨: $^-$) = NO_3^- / (HNO_3 + NO_3

삭제됨: $^+$) = NH_4^+ / (NH_3 + NH_4

Note that OM concentration seems to be increased by both effects of regional transport and local stagnation (Table 2 and Fig. 6f). However, the average estimates of O / C ratio (~0.55) and OM / OC ratio (~1.87), which are in between semi-volatile oxygenated OA (SV-OOA) and low-volatility oxygenated OA (LV-OOA), are similar for the four categorized groups (Table 2). Together with weak correlations of O / C ratio with wind speed ($r = -0.093$) and BLH ($r = -0.172$) in total daily data (n = 118), this suggests that aging and oxidation of SOA in Seoul was not much dependent on external conditions like stagnation or transport. Rather, significant correlations of O / C ratio with temperature ($r = -0.531$) and solar irradiance ($r = -0.370$) indicate the winter-high / summer-low seasonality of the secondary fraction in OA. Such temperature-dependent SOA fraction can be also found in OC / EC ratio ($r = -0.638$ for temperature and $r = -0.469$ for solar irradiance), which can be regarded as an index for secondary OC, and is consistent with partitioning theory (Takekawa et al., 2003).

삭제됨: 4f

3.2 Fractional changes of ALW and SIA by effects of regional transport and local stagnation

The chemical mass fraction of $PM_{2.5}$ are expected to be affected by source characteristics (emissions) and chemical process (secondary aerosol formation), not likely by the physical and dynamical processes (transport and accumulation), which affect the mass concentration of $PM_{2.5}$. Thus, the mass fraction of each component is helpful to understand the source and chemical characteristics of each categorized group.

In terms of the component fraction, $PM_{2.5}$ of the *local stagnation with regional transport* (S-T) group can be characterized by inorganic-rich, wet particles, while that of the *local ventilation with no regional transport* (V-nT) group was relatively organic-richer and drier (Fig. 7). Estimated wet $PM_{2.5}$ (including ALW of both W_i and W_o; $PM_{2.5\ wet}$) of the S-T group contained larger fractions of SIA species (SO_4^{2-}, NO_3^-, and NH_4^+) and ALW but a smaller OM fraction (46% SIA, 23% OM, and 26% ALW) than that of the V-nT group (29% SIA, 43% OM, and 15% ALW). Comparisons with the *local ventilation with regional transport* (V-T) group (37% SIA, 19% OM, and 33% ALW) and the *local stagnation with no regional transport* (S-nT) group (34% SIA, 35% OM, and 21% ALW) groups show that the effect of regional transport increases inorganic and water fractions, while the effect of local stagnation raises organic fraction of the total $PM_{2.5\ wet}$. Note that the increase in ALW fraction from the V-nT (15%) to V-T (33%) groups is much larger than that from the S-nT (21%) to S-T (26%) groups because of the

삭제됨: 5

significantly higher increase in RH from the V-nT (46%) to V-T (61%) groups compared to that from the S-nT (54%) to S-T (52%) groups. The relationship between RH and ALW, as well as hygroscopic properties of the Seoul haze particles, will be further discussed in the next section.

The SO_4^{2-} fraction of dry $PM_{2.5}$ (excluding W_i and W_o; $PM_{2.5\ dry}$) was ~17% for the *no regional transport* (V-nT and S-nT) groups and about 20% and 23% for the V-T and S-T groups, respectively. The SO_4^{2-} fraction in the *no regional transport* groups is close to the background fraction of SO_4^{2-} in $PM_{2.5\ dry}$ in Seoul, and this fraction is comparable to the "local sulfate source" contribution of 21.7% (mostly in the form of ammonium sulfate and equivalent to the SO_4^{2-} contribution of ~16%) identified by the previous source apportionment study on $PM_{2.5}$ in Seoul (Kim et al., 2016). A previous field study conducted on the multiday haze episode showed that the SO_4^{2-} concentration at the upwind background site over the Yellow Sea (Deokjeok Island; 37.233°N, 126.149°E) was nearly the same as the Seoul SO_4^{2-} at the regional-transport stage of haze or the clean period, and even kept ~50% of the Seoul SO_4^{2-} concentration at the local-stagnation stage of the haze episode (Seo et al., 2017). Thus, together with considering the small SO_2 emission in the Seoul metropolitan area compared to the North China Plain (Li et al., 2017; NIER, 2018) and the SO_2 increase by the regional transport effect (*regional transport* groups minus *no regional transport* groups; ~2–4 ppb), the majority of SO_4^{2-} in the *regional transport* (V-T and S-T) groups seems to be directly transported from China or produced during the transport from China before arriving at the Seoul metropolitan area.

삭제됨: SMA

삭제됨: NCP

삭제됨: the NCP

삭제됨: the NCP

삭제됨: SMA

The NO_3^- fraction of $PM_{2.5\ dry}$ was only ~9% for the V-nT group, but increased to 16% and 23% for the S-nT and V-T groups, and reached up to more than 24% for the S-T group. Interestingly, the fractional increase by the local stagnation effect (*local stagnation* groups minus *local ventilation* groups; ~2–7%) is much smaller than that by the regional transport effect (*regional transport* groups minus *no regional transport* groups; ~9–14%) despite the same increase in NO_2 concentration (~15 ppb; Table 2) by two different effects. Seoul is one of the largest sources of NO_x in Korea, but the previous study using satellite NO_x column data with the Lagrangian model demonstrated that the Chinese contribution to the NO_2 columns over Korea reaches up to ~50–70% (Lee et al., 2014). However, the impact of regional transport on the increase in NO_3^- fraction, which is ~2 times higher than that of the local stagnation, indicates a nonlinear effect of regional transport on the NO_3^- increase in the Seoul haze.

The NH_4^+ fraction of $PM_{2.5\ dry}$ was 8% for the V-nT group, 10% for the S-nT group, 13% for the V-T group, and 15% for the S-T group. The higher fractional increase of NH_4^+ by the regional transport effect (T- minus nT-groups; 5%) compared to that by the local stagnation effect (S- minus V-groups; 2%) results from the higher increase in both SO_4^{2-} and NO_3^- aerosols related to the regional transport effect.

삭제됨: more

3.3 Synergistic effect of transported hygroscopic particle on SIA in cold season

The high-concentration, inorganic-rich, and wet particles (high SIA and ALW fractions of $PM_{2.5\ wet}$) mostly belong to the *regional transport* (V-T and S-T) groups, of which backward trajectories originated from the upwind regional source area (the North China Plain and Yangtze River Delta), while relatively low-concentration, organic-rich dry particles (high OM fraction of $PM_{2.5\ wet}$) belong to the *local ventilation with no regional transport* (V-nT) group (Figs. 8a and b). The ALW fraction is a

삭제됨: NCP and YRD

삭제됨: Fig. 6a

function of RH and also increases with the SIA fraction at the same RH (Fig. 8c), similar to the Beijing haze (Wu et al., 2018). This indicates that the Seoul haze is hygroscopic and the major driver of its hygroscopicity is inorganic species. Since the SIA fraction was relatively higher in the *regional transport* groups compared to that in the *no regional transport* groups, the hygroscopic properties of $PM_{2.5}$ in Seoul were more clearly revealed in the *regional transport* groups (Fig. 8d). Therefore, ALW fraction in the transported particles (e.g., the *regional transport* groups) was higher than that in the particles of local origin (e.g., the *local stagnation with no regional transport* (S-nT) group).

The concentrations of SO_4^{2-}, NO_3^-, and NH_4^+ increase with their gas-phase precursors (SO_2, NO_2, and NH_3) in Seoul, except the V-nT group. However, the regression slopes of the SO_4^{2-}, NO_3^-, and NH_4^+ with respect to their precursors in the *regional transport* groups are steeper than the slope of the S-nT group (Fig. 9). Such higher sensitivity of increase in SO_4^{2-}, NO_3^-, and NH_4^+ to the gas-phase precursors of the *regional transport* groups is related to the higher ratios of oxidation (SOR) and partitioning [$\varepsilon(NO_3^-)$ and $\varepsilon(NH_4^+)$] compared to the S-nT group (Figs. 10b, f, and j). Since the average concentrations of total sulfur (= $SO_2 + SO_4^{2-}$), total HNO_3, and total NH_3 are highest in the *local stagnation with regional transport* (S-T) group due to combination of remote precursors transported from China and local precursors accumulated in the stagnant condition (Figs. 10a, e, and i), the high SOR, $\varepsilon(NO_3^-)$, and $\varepsilon(NH_4^+)$ of the *regional transport* groups induced the highest average SO_4^{2-}, NO_3^-, and NH_4^+ concentrations of the S-T group (Table 2).

The SOR, $\varepsilon(NO_3^-)$, and $\varepsilon(NH_4^+)$ averaged for four range classes of temperature and inorganic ALW (W_i) show that all the ratios increased with W_i (Figs. 10d, h, and l), and $\varepsilon(NO_3^-)$ and $\varepsilon(NH_4^+)$ decreased with temperature (Figs. 10g and k). Changes in W_i from the S-nT group (~7 µg m^{-3} in average; $W_{i\,1}$) to the *regional transport* groups (> 20 µg m^{-3} in average; $W_{i\,3}$) increase SOR, $\varepsilon(NO_3^-)$, and $\varepsilon(NH_4^+)$ by approximately up to 20% for each ratio. This implies that the transported haze particles in the *regional transport* groups, which are richer in inorganics and more hygroscopic than the local haze particles of the S-nT group (Fig. 8), promote SIA production. The aqueous-phase oxidation of SO_2 via H_2O_2, O_3, NO_2, and transition metal ion (TMI) pathways (Harris et al., 2013; Cheng et al., 2016; Wang et al., 2016), and the partitioning of HNO_3 and NH_3 via dissolution and dissociation in the wet particles (Seinfeld and Pandis, 2016), are effective ways to produce SO_4^{2-}, NO_3^-, and NH_4^+. Therefore, ALW in the hygroscopic particles can synergistically increase the inorganic species in the precursor-rich urban area like Seoul.

In terms of the synergistic increase in NO_3^- with ALW, the ratio between NO_3^- and SO_4^{2-} can be an important factor. Hygroscopic uptake of ALW by both SO_4^{2-} and NO_3^- can increase pH by dilution effect on hydrogen ions (H^+). Because NO_3^- is a semi-volatile hygroscopic species, the higher pH increased by ALW allows more partitioning of HNO_3 gas into the particle phase and uptakes more ALW. However, if SO_4^{2-} is dominant in the particle, such a feedback process will be weakened because SO_4^{2-} is non-volatile (Guo et al., 2017). The average NO_3^--to-SO_4^{2-} molar ratios of the *regional transport* groups (1.87 for the S-T group and 1.60 for the V-T group) are higher than that of the *no regional transport* groups (1.29 for the S-nT group and 0.81 for the V-nT group). Since ALW, pH, and $\varepsilon(NO_3^-)$ in the *regional transport* (V-T and S-T) groups are higher than those in the *no regional transport* (V-nT and S-nT) groups, this feedback process can explain the synergistic effect of transported particle on the high NO_3^- and ALW fractions.

삭제됨: 6c

삭제됨: 6d

삭제됨: concentration

삭제됨: SIA species (

삭제됨: $^+$) increases

삭제됨: SIA species

삭제됨: 7

삭제됨: SIA species

삭제됨: (

삭제됨: $^+$))

삭제됨: 8b

삭제됨: 8a

삭제됨: SIA concentration

삭제됨: 8d

삭제됨: 8g

삭제됨: 6

삭제됨: SIA species.

삭제됨: SIA

Note that the partitioning of HNO_3 and NH_3 is also dependent on temperature (T) (Figs. 10g and k). Changes in T from the S-nT group (~15°C in average; T_3) to the *regional transport* groups (~9°C in average; T_2) also can increase $\varepsilon(NO_3^-)$ and $\varepsilon(NH_4^+)$ by approximately 20% for each, similar to the effect of inorganic ALW. In Korea, the regional transport of air pollutants from the NCP area is usually accompanied by westerly or northwesterly continental outflow, which induces cold advection, during the cold season (Kim et al., 2018). The colder temperature of the S-T group (~9°C) compared to the S-nT group (~15°C) could help the higher sensitivity of the SIA increase to the precursor concentrations in the S-T group (Fig. 9). Interestingly, the increasing SOR by temperature (and also irradiance) is not significant as much as that by inorganic ALW (Figs. 10c) despite the high-temperature and strong-irradiance conditions conducive to photochemical oxidation of SO_2 in summer. This implies that the observed high SO_4^{2-} in the S-T group resulted not only from the photochemical gas-phase oxidation but also considerably from the aqueous-phase oxidation of SO_2 in the transported wet particles.

삭제됨: 8g
삭제됨: 7
삭제됨: increase
삭제됨: 8c
삭제됨: favorable
삭제됨: for
삭제됨: was induced by
삭제됨: rather than the photochemical gas-phase oxidation

3.4 Effect of NO_x and NH_3 control on mitigating haze pollution in Seoul

The $\varepsilon(NO_3^-)$ can be analytically calculated according to the solubility and dissociation of gas-phase HNO_3, and represented as a sigmoid function (S-curve) of pH (Guo et al., 2018; Nah et al., 2018) by the following equation:

$$\varepsilon(\mathrm{NO_3^-}) = \frac{H^*_{\mathrm{HNO_3}} W_i RT(0.987\times10^{-14})}{\gamma_{\mathrm{H^+}}\gamma_{\mathrm{NO_3^-}}10^{-\mathrm{pH}} + H^*_{\mathrm{HNO_3}} W_i RT(0.987\times10^{-14})} \qquad (2)$$

where 0.987×10^{-14} is the unit conversion factor from atm and µg to SI, R is the gas constant (8.314 J mol^{-1} K^{-1}), W_i (µg m^{-3}) is the ALW content associated with inorganic species, $H^*_{\mathrm{HNO_3}}$ is the effective Henry's law constant (products of Henry's law constant for HNO_3 gases and the acid dissociation constant for $\mathrm{HNO_3} \leftrightarrow \mathrm{NO_3^-} + \mathrm{H^+}$; mol^2 kg^{-2} atm^{-1}) dependent on temperature and pH (Clegg et al., 1998). The product of activity coefficients, $\gamma_{\mathrm{H^+}}\gamma_{\mathrm{NO_3^-}}$, is dependent on both temperature and ionic strength (Kusik and Meissner, 1978; Kim et al., 1993). In this study, daily $\gamma_{\mathrm{H^+}}\gamma_{\mathrm{NO_3^-}}$ were obtained based on daily average ambient temperature and ionic strength from ISORROPIA II, and ranged from 0.135 to 0.734, with an average of 0.333 ± 0.150.

The S-curve of $\varepsilon(NO_3^-)$ as a function of pH is useful for examining the role of inorganic ALW and temperature in HNO_3–NO_3^- partitioning and provides insights into the potential HNO_3 partitioning by change in particle pH. In Fig. 11, both decrease in temperature and increase in ALW can shift the $\varepsilon(NO_3^-)$ curves toward a lower pH, so more HNO_3 can exist in the particle phase. Almost 100% of the total HNO_3 exists in the particle phase at the higher pH (> 4) in Seoul. Since the gas-phase HNO_3 largely formed by the reaction of NO_2 with hydroxyl radicals (OH) is highly water-soluble (Seinfeld and Pandis, 2016), the transported wet particles (the *regional transport* (V-T and S-T) groups) can easily take up HNO_3 gas into the aerosol solution in the NO_x-rich (~60 ppb) environment of Seoul (Vellingiri et al., 2015), particularly during the cold season. Note that ALW can additionally enhance the nitrate radical (NO_3)–N_2O_5 pathway and heterogeneous N_2O_5 hydrolysis (Bertram et al., 2009). In addition, the high NH_3 level (~10 ppb) in Seoul (Phan et al., 2013) helps further to increase the uptake of HNO_3 gas into the aerosol solution (Guo et al., 2018).

삭제됨: 9

To reduce ammonium nitrate aerosols in Seoul, therefore, two ways can be suggested; the NO_x control and the NH_3 control. As shown in Fig. 9b, the observed NO_3^- concentration is highly correlated with the NO_2 level, and this implies that the NO_x control will be an effective way to reduce total HNO_3 and NO_3^- concentrations. Such a direct relationship between NO_x control and nitrate aerosol is significant at the condition of $\varepsilon(NO_3^-)$ close to 1. Because of the higher $\varepsilon(NO_3^-)$ of the transported wet particles, the NO_x reduction will more effectively reduce NO_3^- in the *regional transport* groups compared to the *local stagnation with no regional transport* (S-nT) group. For example, the potential NO_3^- reduction by the 10 ppb decrease of ambient NO_2 concentration deduced from the linear regression in Fig. 9b can be estimated as ~8 µg m^{-3} for the *local ventilation with regional transport* (V-T) group, ~7 µg m^{-3} for the *local stagnation with regional transport* (S-T) group, and ~5 µg m^{-3} for the *local stagnation with no regional transport* (S-nT) group, respectively. On the other hand, the NH_3 control to achieve the low $\varepsilon(NO_3^-)$ by lowering the particle pH from the current level (pH of ~3.5 in average) for the S-T group may cost more than that for the S-nT group, because the $\varepsilon(NO_3^-)$ in the S-nT group (green circles) starts to decrease rapidly at pH < 3.5, while that in the *regional transport* groups (yellow circles for the V-T group and red circles for the S-T group) remains relatively high (~80%) at the lower pH (~2.5) (Fig. 11). Since the haze pollution in Seoul usually becomes severe with the regional transport of hygroscopic wet particles (e.g., the S-T group), more reduction of the NH_3 emissions should be required for the higher-concentration S-T group compared to the lower-concentration S-nT group. However, the benefit of reducing $PM_{2.5}$ mass concentration by NH_3 control can be cancelled out by the adverse effects of strong particle acidity on human health (Fang et al., 2017).

4 Conclusions

Based on $PM_{2.5}$ chemical speciation, gaseous pollutants, and meteorological data in Seoul together with backward trajectory analysis, the present study investigated chemical compositions and characteristics of urban haze particle in the Asian continental outflow region, according to physical and dynamical conditions such as local stagnant condition in the urban area and regional transport of air pollutants from the remote source area. Although various factors like local emissions of primary pollutants and secondary precursors, atmospheric chemistry related to the secondary formation and aging of aerosols, and meteorological conditions can affect the urban haze pollution, a simple categorization by average residence times of backward trajectories within the local (Seoul metropolitan area) and remote (North China Plain and Yangtze River Delta) source areas showed clearly distinguishable characteristics in concentration and fractional composition of $PM_{2.5}$ among the local stagnation / ventilation groups and the regional transport / non-transport groups. In particular, ALW content associated with inorganic species and particle pH estimated by the ISORROPIA II thermodynamic model helped to show different hygroscopic and inorganic partitioning properties of Seoul haze by the categorized groups.

The measurement group of *local stagnation with regional transport* (S-T) from China is characterized by higher $PM_{2.5}$ concentration (72 ± 32 µg m^{-3} of $PM_{2.5\ dry}$) and more inorganic-rich and wetter particles (46% SIA, 23% OM, and 26% ALW in $PM_{2.5\ wet}$) in comparison to the measurement group of *local ventilation with no regional transport* (V-nT; 20 ± 5 µg m^{-3} of

삭제됨: 7b

삭제됨: 7b

삭제됨: 9

삭제됨: SMA

삭제됨: NCP

삭제됨: YRD

$PM_{2.5\ dry}$ and 29% SIA, 43% OM, and 15% ALW in $PM_{2.5\ wet}$). Increase in SIA from the *local ventilation with no regional transport* (V-nT) group to the *local stagnation with regional transport* (S-T) group (~7 times from ~7 to 45 µg m^{-3}) is larger than the OM increase (~2 times from 10 to 23 µg m^{-3}) but relates closely to the increase in inorganic ALW (~8 times from ~3 to 22 µg m^{-3}), indicating inorganic species as a major driver of hygroscopicity. The larger increase in SIA species (SO_4^{2-} from ~3 to 17 µg m^{-3} and NO_3^- from ~2 to 18 µg m^{-3}) compared to the increase in gaseous precursors (SO_2 from 5 to 9 ppb and NO_2 from 27 to 57 ppb) suggests that there is not only the accumulation of local and transported particles but also additional chemical processes for the SIA production in the combination of regional transport and local stagnant conditions.

Further comparisons with the *local stagnation with no regional transport* (S-nT) group and the *local ventilation with regional transport* (V-T) group shows the stronger influence of regional transport rather than local stagnation on the high oxidation and partitioning ratios [SOR, $\varepsilon(NO_3^-)$, and $\varepsilon(NH_4^+)$] associated with the SIA increase. SOR, $\varepsilon(NO_3^-)$, and $\varepsilon(NH_4^+)$ were raised up to ~20% by the increase in inorganic ALW in the Seoul haze condition, and this demonstrates an important role of ALW of the transported hygroscopic particles in increasing of SIA fraction. In addition, $\varepsilon(NO_3^-)$ and $\varepsilon(NH_4^+)$ are decreased by temperature, and thus the transported wet particles can efficiently convert the gas-phase HNO_3 and NH_3 into the particle-phase NO_3^- and NH_4^+ during the cold season. Therefore, the synergistic effect of transported wet particles and local precursors on the SIA increase and high $PM_{2.5}$ concentration in Seoul can be most prominent in the cold season, when the continental outflow dominates East Asia and helps transboundary transport of air pollutants to Korea. Since SO_2 emissions in Seoul are small, the increased SO_4^{2-} in the regional transport condition is likely to be transported from the remote source areas in China or produced during the transport. On the other hand, the high-NO_x (~60 ppb) and NH_3-rich (~10 ppb) conditions in Seoul can promote the uptake of HNO_3 into the wet particle.

Most of the severe haze events in Seoul occur in the local stagnant conditions combined with transport of the preceding regional haze (Seo et al., 2017). The transported regional haze particles with a high inorganic fraction and abundant ALW readily take up HNO_3 and NH_3 gases under the high NO_x and NH_3 conditions of the urban area and consequently reduce the air quality more than local haze formation without regional transport (Fig. 12). Considering both the high $\varepsilon(NO_3^-)$ of the transported wet particles and the low pH required to decrease $\varepsilon(NO_3^-)$ in the combined regional transport–local stagnation condition, NO_x control rather than NH_3 control may be a more effective $PM_{2.5}$ reduction strategy in Seoul.

Our results provide insight into the nonlinear effects of the transported particles and local precursors on urban haze pollution in the regional air quality modeling system. For example, domestic and foreign contributions to PM_{10} concentration over the Seoul metropolitan area estimated by the brute force method approach shows a discrepancy between reductions of domestic and foreign emissions, in particular during the cold season (Kim et al., 2017). The synergistic enhancement of urban haze pollution by the combination of regional and local sources makes precise estimation of domestic and foreign contributions difficult. This study also shows need for international cooperation in air quality management.

삭제됨: (

삭제됨: $^+$))

삭제됨: 10

삭제됨: SMA

삭제됨: (BFM)

Code availability

ISORROPIA II is available at: https://isorropia.epfl.ch/code-repository/. HYSPLIT model is available at: https://www.ready.noaa.gov/HYSPLIT.php.

Data availability

Daily $PM_{2.5}$ measurements, chemical analysis, meteorological factors and ISORROPIA II results data utilized in this study are available at: https://drive.google.com/open?id=1hJrwViP_qx23dTuBxLapbWhAn5LrTXMI. The hourly data of SO_2, NO_2, CO, O_3, and PM_{10} concentrations at 34 air quality monitoring sites in Seoul for the analysis period are available on the website managed by the Korea Environment Corporation (2020; https://www.airkorea.or.kr/web/last_amb_hour_data?pMENU_NO=123). The hourly meteorological data of temperature, sea level pressure, relative humidity, wind speed, and solar irradiance at the Seoul weather station for the same period can be found on the website of the KMA (2020; https://data.kma.go.kr/data/grnd/selectAsosRltmList.do?pgmNo=36). The ERA-Interim data (Dee et al., 2011) can be accessed via the European Centre for Medium-Range Weather Forecasts (ECMWF) data server (http://apps.ecmwf.int/datasets/data/interim-full-daily/).

삭제됨: https://drive.google.com/open?id=1LfH0hNqtSDIoQmtqWgCw0lagbFu6LLYJ.

삭제됨: 2019

삭제됨: 2019

Author contributions

JS initiated the investigation and performed thermodynamic modeling analyses. JS and YBL extensively discussed the concept. HCJ conducted the field measurement and provided chemical analyses. DY and JYK provided additional feedback on the manuscript. JS prepared the manuscript with contributions from all co-authors.

Competing interests

The authors declare that they have no conflict of interest.

Acknowledgements

This research was supported by the Korea Institute of Science and Technology (KIST) and the National Strategic Project - Fine Particle of the National Research Foundation of Korea (NRF) funded by the Ministry of Science and ICT (MSIT), the Ministry of Environment (ME), and the Ministry of Health and Welfare (MOHW) (2017M3D8A1090654). Yong Bin Lim was supported by NRF (2019M3D8A1070941). Daeok Youn was supported by the Basic Science Research Program through the National Research Foundation of Korea (NRF) funded by the Ministry of Education (2015R1D1A3A01020130) and Korea Environment Industry & Technology Institute (KEITI) funded by Korea Ministry of Environment (MOE) (2018001310004).

References

Asa-Awuku, A., Nenes, A., Gao, S., Flagan, R. C., and Seinfeld, J. H.: Water-soluble SOA from Alkene ozonolysis: composition and droplet activation kinetics inferences from analysis of CCN activity, Atmos. Chem. Phys., 10, 1585–1597, https://doi.org/10.5194/acp-10-1585-2010, 2010.

Ashbaugh, L. L. and Eldred R. A.: Loss of particle nitrate from Teflon sampling filters: Effects on measured gravimetric mass in California and in the IMPROVE network, J. Air Waste Manage. Assoc., 54, 93–104, https://doi.org/10.1080/10473289.2004.10470878, 2004.

Bertram, T. H., Thornton, J. A., Riedel, T. P., Middlebrook, A. M., Bahreini, R., Bates, T. S., Quinn, P. K., and Coffman, D. J.: Direct observations of N_2O_5 reactivity on ambient aerosol particles, Geophys. Res. Lett., 36, L19803, https://doi.org/10.1029/2009GL040248, 2009.

Birch, M. and Cary, R: Elemental carbon-based method for monitoring occupational exposures to particulate diesel exhaust, Aerosol Sci. Technol., 25, 221–241, https://doi.org/10.1080/02786829608965393, 1996.

Carlton, A. G. and Turpin, B. J.: Particle partitioning potential of organic compounds is highest in the Eastern US and driven by anthropogenic water, Atmos. Chem. Phys., 13, 10203–10214, https://doi.org/10.5194/acp-13-10203-2013, 2013.

Chang, R. Y.-W., Slowik, J. G., Shantz, N. C., Vlasenko, A., Liggio, J., Sjostedt, S. J., Leaitch, W. R., and Abbatt, J. P. D.: The hygroscopicity parameter (κ) of ambient organic aerosol at a field site subject to biogenic and anthropogenic influences: relationship to degree of aerosol oxidation, Atmos. Chem. Phys., 10, 5047–5064, https://doi.org/10.5194/acp-10-5047-2010, 2010.

Cheng, Y., Zheng, G., Wei, C., Mu, Q., Zheng, B., Wang, Z., Gao, M., Zhang, Q., He, K., Carmichael, G., Pöschl, U., and Su, H: Reactive nitrogen chemistry in aerosol water as a source of sulfate during haze events in China, Sci. Adv., 2, e1601530, https://doi.org/10.1126/sciadv.1601530, 2016.

Chow, J. C., Watson, J. G., Lowenthal, D. H., and Magliano, K. L.: Loss of $PM_{2.5}$ nitrate from filter samples in central California, J. Air Waste Manage. Assoc., 55, 1158–1168, https://doi.org/10.1080/10473289.2005.10464704, 2005.

Clegg, S. L., Brimblecombe, P., and Wexler, A. S.: Thermodynamic model of the system $H^+–NH_4^+– SO_4^{2-}–NO_3^-–H_2O$ at tropospheric temperatures, J. Phys. Chem. A, 102, 2137–2154, https://doi.org/10.1021/jp973042r, 1998.

Dee, D. P., Uppala, S. M., Simmons, A. J., Berrisford, P., Poli, P., Kobayashi, S., Andrae, U., Balmaseda, M. A., Balsamo, G., Bauer, P., Bechtold, P., Beljaars, A. C. M., van de Berg, L., Bidlot, J., Bormann, N., Delsol, C., Dragani, R., Fuentes, M., Geer, A. J., Haimberger, L., Healy, S. B., Hersbach, H., Hólm, E. V., Isaksen, L., Kållberg, P., Köhler, M., Matricardi, M., McNally, A. P., Monge-Sanz, B. M., Morcrette, J.-J., Park, B.-K., Peubey, C., de Rosnay, P., Tavolato, C., Thépaut, J.-N., and Vitart, F.: The ERA-Interim reanalysis: configuration and performance of the data assimilation system, Q. J. Roy. Meteor. Soc., 137, 553–597, https://doi.org/10.1002/qj.828, 2011.

Fang, T., Guo, H., Zeng, L., Verma, V., Nenes, A., and Weber, R. J.: Highly Acidic Ambient Particles, Soluble Metals, and Oxidative Potential: A Link between Sulfate and Aerosol Toxicity, Environ. Sci. Technol., 51, 2611–2620, https://doi.org/10.1021/acs.est.6b06151, 2017.

Fountoukis, C. and Nenes, A.: ISORROPIA II: A computationally efficient thermodynamic equilibrium model for K^+–Ca^{2+}–Mg^{2+}–NH_4^+–Na^+–SO_4^{2-}–NO_3^-–Cl^-–H_2O aerosols, Atmos. Chem. Phys., 7, 4639–4659, https://doi.org/10.5194/acp-7-4639-2007, 2007.

Guo, H., Liu, J., Froyd, K. D., Roberts, J. M., Veres, P. R., Hayes, P. L., Jimenez, J. L., Nenes, A., and Weber, R. J.: Fine particle pH and gas–particle phase partitioning of inorganic species in Pasadena, California, during the 2010 CalNex campaign, Atmos. Chem., Phys., 17, 5703–5719, https://doi.org/10.5194/acp-17-5703-2017, 2017.

Guo, H., Otjes, R., Schlag, P., Kiendler-Scharr, A., Nenes, A., and Weber, R. J.: Effectiveness of ammonia reduction on control of fine particle nitrate, Atmos. Chem. Phys., 18, 12241–12256, https://doi.org/10.5194/acp-18-12241-2018, 2018.

Harris, E., Sinha, B., van Pinxteren, D., Tilgner, A., Fomba, K. W., Schneider, J., Roth, A., Gnauk, T., Fahlbusch, B., Mertes, S., Lee, T., Collett, J., Foley, S., Borrmann, S., Hoppe, P., and Herrmann, H.: Enhanced role of transition metal ion catalysis during in-cloud oxidation of SO_2, Science, 340, 727–730, https://doi.org/10.1126/science.1230911, 2013.

Hennigan, C. J., Izumi, J., Sullivan, A. P., Weber, R. J., and Nenes, A.: A critical evaluation of proxy methods used to estimate the acidity of atmospheric particles, Atmos. Chem. Phys., 15, 2775–2790, https://doi.org/10.5194/acp-15-2775-2015, 2015.

Kim, B., Seo, J., Kim, J. Y., Lee, J. Y., and Kim, Y.: Transported vs. local contributions from secondary and biomass burning sources to $PM_{2.5}$, Atmos. Environ., 144, 24–36, https://doi.org/10.1016/j.atmosenv.2016.08.072, 2016.

Kim, H. C., Kim, E., Bae, C., Cho, J. H., Kim, B.-U., and Kim, S.: Regional contributions to particulate matter concentration in the Seoul metropolitan area, South Korea: seasonal variation and sensitivity to meteorology and emissions inventory, Atmos. Chem. Phys., 17, 10315–10332, https://doi.org/10.5194/acp-17-10315-2017, 2017.

Kim, Y., Seo, J., Kim, J. Y., Lee, J. Y., Kim, H., and Kim, B. M.: Characterization of $PM_{2.5}$ and identification of transported secondary and biomass burning contribution in Seoul, Korea, Environ. Sci. Pollut. Res., 25, 4330–4343, https://doi.org/10.1007/s11356-017-0772-x: 2018.

Kim, Y. P., Seinfeld, J. H., and Saxena, P.: Atmospheric gas-aerosol equilibrium I. Thermodynamic model, Aerosol Sci. Technol., 19, 157–181, https://doi.org/10.1080/02786829308959628, 1993.

Kim, Y. P. and Lee, G.: Trend of air quality in Seoul: policy and science, Aerosol Air Qual. Res., 18, 2141–2156, https://doi.org/10.4209/aaqr.2018.03.0081, 2018.

KMA (Korea Meteorological Administration): Automated Synoptic Observing System (ASOS) data, available at: https://data.kma.go.kr/data/grnd/selectAsosRltmList.do?pgmNo=36, last access: 23 October 2019.

Korea Environment Corporation: Data from the NIER air quality monitoring sites, available at: https://www.airkorea.or.kr/web/last_amb_hour_data?pMENU_NO=123, last access: 23 October 2019.

Kusik, C. L. and Meissner H. P.: Electrolyte activity coefficients in inorganic processing, AIChE Symposium Series, 173, 14–20, 1978.

Lee, H.-J., Kim, S.-W., Brioude, J., Cooper, O. R., Frost, G. J., Kim, C.-H., Park, R. J., Trainer, M., and Woo, J.- H.: Transport of NOx in East Asia identified by satellite and in situ measurements and Lagrangian particle dispersion model simulations, J. Geophys. Res., 119, 2574–2596, https://doi.org/10.1002/2013JD021185, 2014.

Li, M., Zhang, Q., Kurokawa, J., Woo, J.-H., He, K., Lu, Z., Ohara, T., Song, Y., Streets, D. G., Carmichael, G. R., Cheng, Y., Hong, C., Huo, H., Jiang, X., Kang, S., Liu, F., Su, H., and Zheng, B.: MIX: a mosaic Asian anthropogenic emission inventory under the international collaboration framework of the MICS-Asia and HTAP, Atmos. Chem. Phys., 17, 935–963, https://doi.org/10.5194/acp-17-935-2017, 2017.

Lim, Y. B., Seo, J., Kim, J. Y., Kim, Y. P., and Jin, H. C.: Local formation of sulfates contributes to the urban haze with regional transport origin, Environ. Res. Lett., https://doi.org/10.1088/1748-9326/ab83aa, in press, 2020.

Liu, Y., Wu, Z., Wang, Y., Xiao, Y., Gu, F., Zheng, J., Tan, T., Shang, D., Wu, Y., Zeng, L., Hu, M., Bateman, A. P., and Martin, S. T.: Submicrometer particles are in the liquid state during heavy haze episodes in the urban atmosphere of Beijing, China, Environ. Sci. Technol. Lett., 4, 427–432, https://doi.org/10.1021/acs.estlett.7b00352, 2017.

Marais, E. A., Jacob, D. J., Jimenez, J. L., Campuzano-Jost, P., Day, D. A., Hu, W., Krechmer, J., Zhu, L., Kim, P. S., Miller, C. C., Fisher, J. A., Travis, K., Yu, K., Hanisco, T. F., Wolfe, G. M., Arkinson, H. L., Pye, H. O. T., Froyd, K. D., Liao, J., and McNeill, V. F.: Aqueous-phase mechanism for secondary organic aerosol formation from isoprene: application to the southeast United States and co-benefit of SO_2 emission controls, Atmos. Chem. Phys., 16, 1603–1618, https://doi.org/10.5194/acp-16-1603-2016, 2016.

McNeill, V. F.: Aqueous organic chemistry in the atmosphere: sources and chemical processing of organic aerosols, Environ. Sci. Technol., 49, 1237–1244, https://doi.org/10.1021/es5043707, 2015.

Nah, T., Guo, H., Sullivan, A. P., Chen, Y., Tanner, D. J., Nenes, A., Russell, A., Ng, N. L., Huey, L. G., and Weber, R. J.: Characterization of aerosol composition, aerosol acidity, and organic acid partitioning at an agriculturally intensive rural southeastern US site, Atmos. Chem. Phys., 18, 11471–11491, https://doi.org/10.5194/acp-18-11471-2018, 2018.

Nie, W., Wang, T., Gao, X., Pathak, R. K., Wang, X., Gao, R., Zhang, Q., Yang, L., and Wang, W.: Comparison among filter-based, impactor-based and continuous techniques for measuring atmospheric fine sulfate and nitrate, Atmos. Environ., 44, 4396–4403, https://doi.org/10.1016/j.atmosenv.2010.07.047, 2010.

NIER (National Institute of Environmental Research): National air pollutants emission 2015 (NIER-GP2017-210), NIER, Incheon, South Korea, available at: http://webbook.me.go.kr/DLi-File/NIER/09/023/5668670.pdf (last access: 21 October 2019), 2018 (in Korean).

Nguyen, T. K. V., Capps, S. L., and Carlton, A. G.: Decreasing aerosol water is consistent with OC trends in the Southeast U.S., Environ. Sci. Technol., 49, 7843–7850, https://doi.org/10.1021/acs.est.5b00828, 2015.

Nguyen, T. K. V., Zhang, Q., Jimenez, J. L., Pike, M., and Carlton, A. G.: Liquid water: ubiquitous contributor to aerosol mass, Environ. Sci. Technol. Lett., 3, 257–263, https://doi.org/10.1021/acs.estlett.6b00167, 2016.

삭제됨: et

Phan, N.-T., Kim, K.-H., Shon, Z.-H., Jeon, E.-C., Jung, K., and Kim, N.-J.: Analysis of ammonia variation in the urban atmosphere, Atmos. Environ., 65, 177–185, https://doi.org/10.1016/j.atmosenv.2012.10.049, 2013.

Pope, C. A. and Dockery, D. W.: Health effects of fine particulate air pollution: lines that connect, J. Air Waste Manage. Assoc., 56, 709–742, https://doi.org/10.1080/10473289.2006.10464485, 2006.

Seinfeld, J. H. and Pandis, S. N.: Atmospheric Chemistry and Physics: From Air Pollution to Climate Change, 3rd Edn., John Wiley & Sons, Inc., Hoboken, New Jersey, 2016.

Seo, J., Kim, J. Y., Youn, D., Lee, J. Y., Kim, H., Lim, Y. B., Kim, Y., and Jin, H. C.: On the multiday haze in the Asian continental outflow: the important role of synoptic conditions combined with regional and local sources, Atmos. Chem. Phys., 17, 9311–9332, https://doi.org/10.5194/acp-17-9311-2017, 2017.

Seo, J., Park, D.-S. R., Kim, J. Y., Youn, D., Lim, Y. B., and Kim, Y.: Effects of meteorology and emissions on urban air quality: a quantitative statistical approach to long-term records (1999–2016) in Seoul, South Korea, Atmos. Chem. Phys., 18, 16121–16137, https://doi.org/10.5194/acp-18-16121-2018, 2018.

Song, S., Gao, M., Xu, W., Shao, J., Shi, G., Wang, S., Wang, Y., Sun, Y., and McElroy, M. B.: Fine-particle pH for Beijing winter haze as inferred from different thermodynamic equilibrium models, Atmos. Chem. Phys., 18, 7423–7438, https://doi.org/10.5194/acp-18-7423-2018, 2018.

Stein, A. F., Draxler, R. R., Rolph, G. D., Stunder, B. J. B., Cohen, M. D., and Ngan, F.: NOAA's HYSPLIT atmospheric transport and dispersion modeling system, Bull. Am. Meteorol. Soc., 96, 2059–2077, https://doi.org/10.1175/BAMS-D-14-00110.1, 2015.

Stokes, R. H. and Robinson, R. A.: Interactions in aqueous nonelectrolyte solutions. I. Solute-solvent equilibria, J. Phys. Chem., 70, 2126–2131, https://doi.org/10.1021/j100879a010, 1966.

Sun, Y., Jiang, Q., Wang, Z., Fu, P., Li, J., Yang, T., and Yin, Y.: Investigation of the source and evolution processes of severe haze pollution in Beijing in January 2013, J. Geophys. Res. Atmos., 119, 4380–4398, https://doi.org/10.1002/2014JD021641, 2014.

Takekawa, H., Minoura, H., and Yamazaki S.: Temperature dependence of secondary organic aerosol formation by photo-oxidation of hydrocarbons, Atmos. Environ., 37, 3413–3424, https://doi.org/10.1016/S1352-2310(03)00359-5, 2003.

Tie, X., Huang, R.-J., Cao, J., Zhang, Q., Cheng, Y., Su, H., Chang, D., Pöschl, U., Hoffmann, T., Dusek, U., Li, G., Worsnop, D. R., and O'Dowd, C. D.: Severe pollution in China amplified by atmospheric moisture, Sci. Rep., 7, 15760, https://doi.org/10.1038/s41598-017-15909-1, 2017.

Turpin, B. J. and Lim, H.-J.: Species contributions to $PM_{2.5}$ mass concentrations: revisiting common assumptions for estimating organic mass, Aerosol Sci. Tech., 35, 602–610, https://doi.org/10.1080/02786820152051454, 2001.

van der A, R. J., Mijling, B., Ding, J., Koukouli, M. E., Liu, F., Li, Q., Mao, H., and Theys, N.: Cleaning up the air: Effectiveness of air quality policy for SO_2 and NO_x emissions in China, Atmos. Chem. Phys., 17, 1775–1789, https://doi.org/10.5194/acp-17-1775-2017, 2017.

Vellingiri, K., Kim, K.-H., Jeon, J. Y., Brown, R. J. C., and Jung, M.-C.: Changes in NO_x and O_3 concentrations over a decade at a central urban area of Seoul, Korea, Atmos. Environ., 112, 116–125, https://doi.org/10.1016/j.atmosenv.2015.04.032, 2015.

Wang, H., Lu, K., Chen, X., Zhu Q., Chen, Q., Guo, S., Jiang, M., Li, X., Shang, D., Tan, Z., Wu, Y., Wu, Z., Zou, Q., Zheng, Y., Zeng, L., Zhu, T., Hu, M., and Zhang, Y.: High N_2O_5 concentrations observed in urban Beijing: implications of a large nitrate formation pathway, Environ. Sci. Technol. Lett., 4, 416–420, https://doi.org/10.1021/acs.estlett.7b00341, 2017.

Wang, G., Zhang, R., Gomez, M. E., Yang, L., Zamora, M. L., Hu, M., Lin, Y., Peng, J., Guo, S., Meng, J., Li, J., Cheng, C., Hu, T., Ren, Y., Wang, Y., Gao, J., Cao, J., An, Z., Zhou, W., Li, G., Wang, J., Tian, P., Marrero-Ortiz, W., Secrest, J., Du, Z., Zheng, J., Shang, D., Zeng, L., Shao, M., Wang, W., Huang, Y., Wang, Y., Zhu, Y., Li, Y., Hu, J., Pan, B., Cai, L., Cheng, Y., Ji, Y., Zhang, F., Rosenfeld, D., Liss, P. S., Duce, R. A., Kolb, C. E., and Molina M. J.: Persistent sulfate formation from London fog to Chinese haze, Proc. Natl Acad. Sci. USA, 113, 13630–13635, https://doi.org/10.1073/pnas.1616540113, 2016.

Weber, R. J., Guo, H., Russell, A. G., and Nenes, A.: High aerosol acidity despite declining atmospheric sulfate concentrations over the past 15 years, Nat. Geosci., 9, 282–285, https://doi.org/10.1038/ngeo2665, 2016.

Wu, Z., Wang, Y., Tan, T., Zhu, Y., Li, M., Shang, D., Wang, H., Lu, K., Guo, S., Zeng, L., and Zhang, Y.: Aerosol liquid water driven by anthropogenic inorganic salts: Implying its key role in haze formation over the North China Plain, Environ. Sci. Technol. Lett., 5, 160–166, https://doi.org/10.1021/acs.estlett.8b00021, 2018.

Zhang, R., Wang, G., Guo, S., Zamora, M. L., Ying, Q., Lin, Y., Wang, W., Hu, M., and Wang, Y: Formation of urban fine particulate matter, Chem. Rev., 115, 3803–3855, https://doi.org/10.1021/acs.chemrev.5b00067, 2015.

Zheng, G. J., Duan, F. K., Su, H., Ma, Y. L., Cheng, Y., Zheng, B., Zhang, Q., Huang, T., Kimoto, T., Chang, D., Pöschl, U., Cheng, Y. F., and He, K. B.: Exploring the severe winter haze in Beijing: the impact of synoptic weather, regional transport and heterogeneous reactions, Atmos. Chem. Phys., 15, 2969–2983, https://doi.org/10.5194/acp-15-2969-2015, 2015.

Table 1: List of four categorized groups of daily $PM_{2.5}$ measurements in this study.

Categories	Acronyms	Trajectory residence time in the Chinese source area (t_{CHN})	Trajectory residence time in the Seoul metropolitan area (t_{SMA})
Local ventilation with no regional transport	V-nT	$t_{CHN} = 0$ h	$t_{SMA} < 6$ h
Local stagnation with no regional transport	S-nT	$t_{CHN} = 0$ h	$t_{SMA} \geq 6$ h
Local ventilation with regional transport	V-T	$t_{CHN} \geq 6$ h	$t_{SMA} < 6$ h
Local stagnation with regional transport	S-T	$t_{CHN} \geq 6$ h	$t_{SMA} \geq 6$ h

Table 2: The average and standard deviation of PM$_{2.5}$ chemical composition, meteorological factors, related gas concentrations, thermodynamic model results and gas-particle partitioning ratios, and mass concentration ratios to wet PM$_{2.5}$ (PM$_{2.5\ \mathrm{wet}}$) for the *local ventilation with no regional transport* (V-nT) group, the *local stagnation with no regional transport* (S-nT) group, the *local ventilation with regional transport* (V-T) group, and the *local stagnation with regional transport* (S-T) group, and *p*-values derived from Welch's *t*-test for the composite differences between the S-T and S-nT groups and between the S-T and V-T groups.

Components	Units	Composite average and standard deviation				*p*-values from Welch's *t*-test	
		[V-nT] ($n = 9$)	[S-nT] ($n = 15$)	[V-T] ($n = 15$)	[S-T] ($n = 21$)	[S-T] minus [S-nT] (Transport effect)	[S-T] minus [V-T] (Stagnation effect)
Meteorological factors							
T	(°C)	2.6 ± 13.2	15.2± 11.5	9.4 ± 6.0	9.3 ± 8.5	$p = 0.104$	$p = 0.967$
RH	(%)	45.9 ± 10.0	53.5 ± 10.2	61.0 ± 9.3	51.8 ± 11.7	$p = 0.632$	$p = 0.013$
WS	(m s^{-1})	3.5 ± 0.7	2.4 ± 0.6	3.2 ± 0.9	2.4 ± 0.7	$p = 0.824$	$p = 0.009$
SI	(W m^{-2})	167 ± 41	172 ± 53	154 ± 64	137 ± 67	$p = 0.094$	$p = 0.445$
BLH [a]	(m)	770 ± 177	550 ± 210	666 ± 277	457 ± 165	$p = 0.165$	$p = 0.016$
Gaseous species							
SO$_2$	(ppb)	4.6 ± 0.6	5.2 ± 2.0	6.6 ± 2.2	8.8 ± 2.7	$p < 0.001$	$p = 0.012$
NO$_2$	(ppb)	27.4 ± 4.1	41.6 ± 11.7	41.2 ± 9.5	57.3 ± 12.5	$p < 0.001$	$p < 0.001$
CO	(ppm)	0.42 ± 0.05	0.55 ± 0.26	0.66 ± 0.28	0.89 ± 0.31	$p = 0.001$	$p = 0.026$
O$_3$	(ppb)	24.6 ± 7.0	20.1 ± 11.9	23.1 ± 10.5	15.5 ± 9.0	$p = 0.219$	$p = 0.031$
NH$_3$ [b]	(ppb)	4.9 ± 4.1	10.5 ± 3.0	10.2 ± 3.4	11.0 ± 4.3	$p = 0.668$	$p = 0.499$
PM$_{2.5}$ components							
PM$_{2.5\ \mathrm{dry}}$	(μg m^{-3})	19.9 ± 4.8	34.4 ± 20.7	53.3 ± 33.7	72.2 ± 31.9	$p < 0.001$	$p = 0.100$
SO$_4^{2-}$	(μg m^{-3})	3.3 ± 0.7	5.8 ± 4.1	10.8 ± 7.6	16.7 ± 11.2	$p < 0.001$	$p = 0.069$
NO$_3^-$	(μg m^{-3})	1.7 ± 1.4	5.4 ± 7.3	12.1 ± 11.2	17.6 ± 12.1	$p < 0.001$	$p = 0.166$
NH$_4^+$	(μg m^{-3})	1.6 ± 0.5	3.4 ± 3.6	6.9 ± 5.7	10.8 ± 6.9	$p < 0.001$	$p = 0.075$
EC	(μg m^{-3})	1.4 ± 0.6	1.7 ± 0.6	1.6 ± 0.6	2.1 ± 0.8	$p = 0.128$	$p = 0.036$
OM	(μg m^{-3})	10.1 ± 4.4	15.3 ± 10.1	15.0 ± 7.0	22.9 ± 8.6	$p = 0.025$	$p = 0.005$
W_i	(μg m^{-3})	2.7 ± 1.4	7.4 ± 7.5	23.7 ± 24.9	22.2 ± 18.6	$p = 0.003$	$p = 0.853$
W_o	(μg m^{-3})	0.9 ± 0.4	2.2 ± 1.7	3.1 ± 2.7	3.3 ± 2.3	$p = 0.087$	$p = 0.833$
Carbonaceous analysis							
O / C	(atomic ratio)	0.55 ± 0.11	0.55 ± 0.07	0.54 ± 0.04	0.55 ± 0.07	$p = 0.883$	$p = 0.622$
OM / OC	(mass ratio)	1.87 ± 0.15	1.87 ± 0.10	1.86 ± 0.05	1.87 ± 0.08	$p = 0.927$	$p = 0.632$
OC / EC	(mass ratio)	4.2 ± 1.7	4.8 ± 2.4	5.7 ± 2.5	6.2 ± 2.1	$p = 0.071$	$p = 0.510$
ISORROPIA II analysis							
Ionic strength	(M)	54.3 ± 16.2	42.2 ± 17.6	30.6 ± 10.3	47.1 ± 22.7	$p = 0.470$	$p = 0.006$
pH		3.1 ± 0.6	3.2 ± 0.7	3.5 ± 0.5	3.5 ± 0.7	$p = 0.186$	$p = 0.808$
Oxidation / Partitioning							
SOR	(molar ratio)	0.13 ± 0.04	0.19 ± 0.07	0.25 ± 0.09	0.28 ± 0.12	$p = 0.006$	$p = 0.439$
$\varepsilon(\mathrm{NO_3^-})$	(molar ratio)	0.83 ± 0.28	0.67 ± 0.31	0.93 ± 0.09	0.90 ± 0.19	$p = 0.017$	$p = 0.481$
$\varepsilon(\mathrm{NH_4^+})$	(molar ratio)	0.40 ± 0.27	0.25 ± 0.14	0.43 ± 0.18	0.52 ± 0.18	$p < 0.001$	$p = 0.150$

[a] Reanalysis data from the ERA-Interim at 37.5°N, 127.0°E. [b] Statistically reconstructed data based on Phan et al. (2013).

T: temperature; RH: relative humidity; WS: wind speed; SI: solar irradiance; BLH: boundary layer height; EC: elemental carbon; OM: organic matter; W_i: aerosol liquid water (ALW) content associated with inorganic species; W_o: ALW content associated with OM; OC: organic carbon; SOR: sulfur oxidation ratio; $\varepsilon(\mathrm{NO_3^-})$: nitrate partitioning ratio; $\varepsilon(\mathrm{NH_4^+})$: ammonium partitioning ratio.

삭제됨: 3.6 ± 2.8
삭제됨: 7…0.5 ± 2.1
삭제됨: 7.5 ± …0.2.6
삭제됨: 8.2 ± 3
삭제됨: 470
삭제됨: 481
삭제됨: 6… ± 1.3
삭제됨: 1
삭제됨: 4… ± 24.7
삭제됨: 0… ± 18.5
삭제됨: 851
삭제됨: 086
삭제됨: 817
삭제됨: 52…4.3 ± 16.2 ± 15.4
삭제됨: 41.5…2.2 ± 17.2
삭제됨: 2 ± 9.9
삭제됨: 46.6…7.1 ± 22.6
삭제됨: 448
삭제됨: 3
삭제됨: 3
삭제됨: 4
삭제됨: 6… ± 0.6
삭제됨: 195
삭제됨: 657
삭제됨: 12
삭제됨: 17
삭제됨: 24
삭제됨: 27
삭제됨: 005
삭제됨: 480
삭제됨: 29
삭제됨: 94
삭제됨: 016
삭제됨: 492
삭제됨: 33…0 ± 0.19
삭제됨: 23
삭제됨: 41
삭제됨: 50…2 ± 0.19
삭제됨: 178

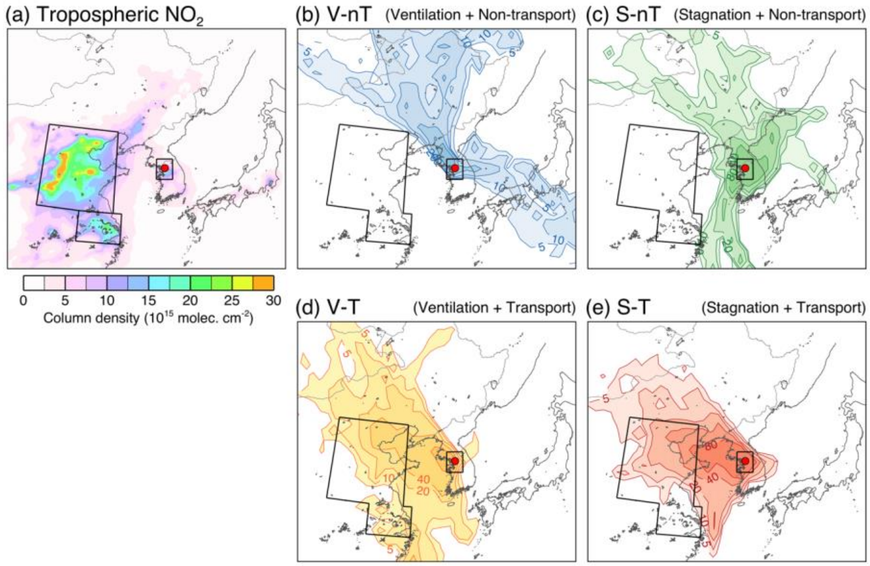

Figure 1: (a) Tropospheric NO_2 column density obtained from the Ozone Monitoring Instrument (OMI) onboard the EOS-Aura satellite, averaged for 2012–2014, and the major anthropogenic emission areas defined in this study (North China Plain [NCP]: 112°E –121°E, 33°N –41°N; Yangtze River Delta [YRD]: 117°E –122°E, 30°N –33°N; and Seoul metropolitan area [SMA]; 126°E –128°E, 36.5°N –38.5°N). (b–e) Trajectory frequency (number of endpoints in each 1° × 1° grid cell per number of trajectories, %) derived from the HYSPLIT 72-h backward trajectories obtained 500 m above the Korea Institute of Science and Technology (KIST) site and average chemical compositions of particulate matter under 2.5 µm in diameter ($PM_{2.5}$) for the (b) *local ventilation with no regional transport* (V-nT) group, (c) *local stagnation with no regional transport* (S-nT) group, (d) *local ventilation with regional transport* (V-T) group, and (e) *local stagnation with regional transport* (S-T) group. Seoul is marked with a solid red circle.

삭제됨**: Metropolitan Area**

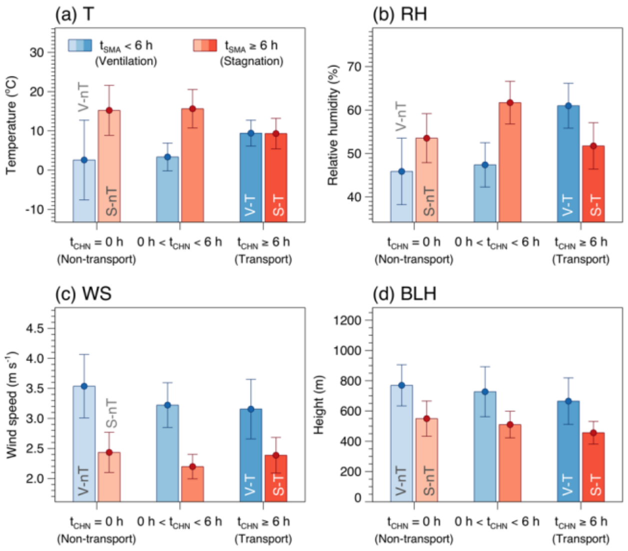

Figure 2: Averages and confidence intervals at 95% of (a) temperature (*T*), (b) relative humidity (RH), (c) wind speed (WS), and (d) boundary layer height (BLH) for the six case groups categorized by the ranges of the average daily residence time of backward trajectories in the Seoul metropolitan area (t_{SMA}) and in the North China Plain and Yangtze River Delta (t_{CHN}).

삭제됨: SMA

삭제됨: NCP

삭제됨: YRD

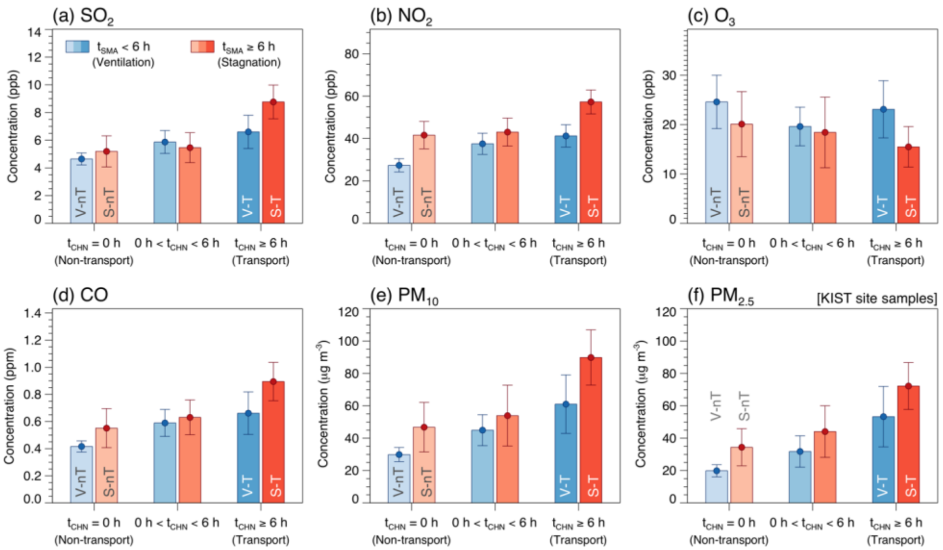

Figure 3: Averages and confidence intervals at 95% of daily average concentrations of (a) SO_2, (b) NO_2, (c) O_3, (d) CO, and (e) PM_{10}, together with (f) $PM_{2.5}$ measured at the KIST site in this study (dry $PM_{2.5}$) for the six case groups categorized by ranges of the average daily residence time of backward trajectories in the Seoul metropolitan area (t_{SMA}) and in the North China Plain and Yangtze River Delta (t_{CHN}).

삭제됨: SMA

삭제됨: NCP

삭제됨: YRD

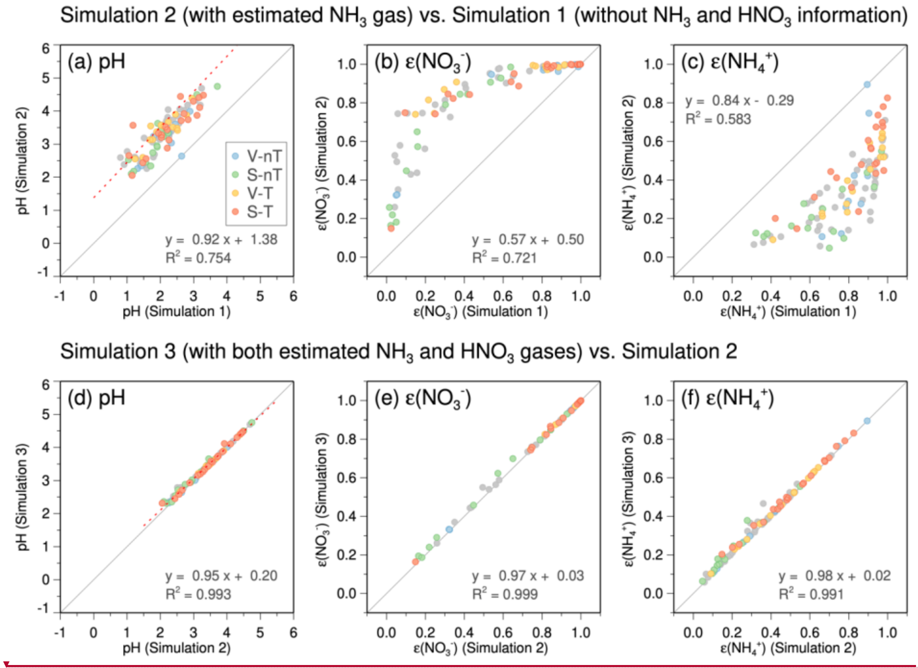

Figure 4: Comparisons of the predicted pH, nitrate partitioning ratio [ε(NO_3^-) = NO_3^- / (HNO_3 + NO_3^-)], and ammonium partitioning ratio [ε(NH_4^+) = NH_4^+ / (NH_3 + NH_4^+)] between (a–c) the simulation without gas-phase NH_3 and HNO_3 information (using NH_4^+ and NO_3^- as the total NH_3 and total HNO_3; Simulation 1) and the simulation with reconstructed NH_3 (using NH_3 + NH_4^+ as the total NH_3 but only NO_3^- as the total HNO_3; Simulation 2) and (d–f) the Simulation 2 and the simulation with both estimated gas-phase NH_3 and HNO_3 information (this study; Simulation 3). Filled circles in light blue, light green, light yellow, and light red colors represent daily data belong to the *local ventilation with no regional transport* (V-nT) group, *local stagnation with no regional transport* (S-nT) group, *local ventilation with regional transport* (V-T) group, and *local stagnation with regional transport* (S-T) group, respectively. Gray solid lines indicate a 1-to-1 relationship.

삭제됨:
Figure 4

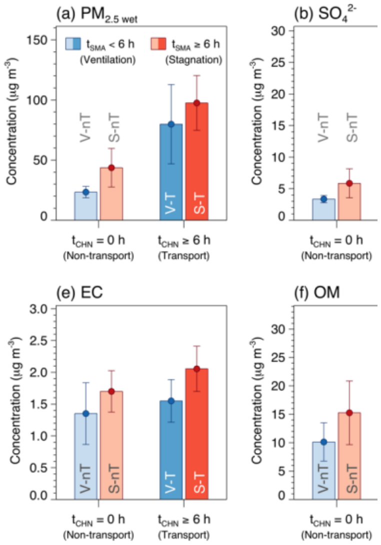

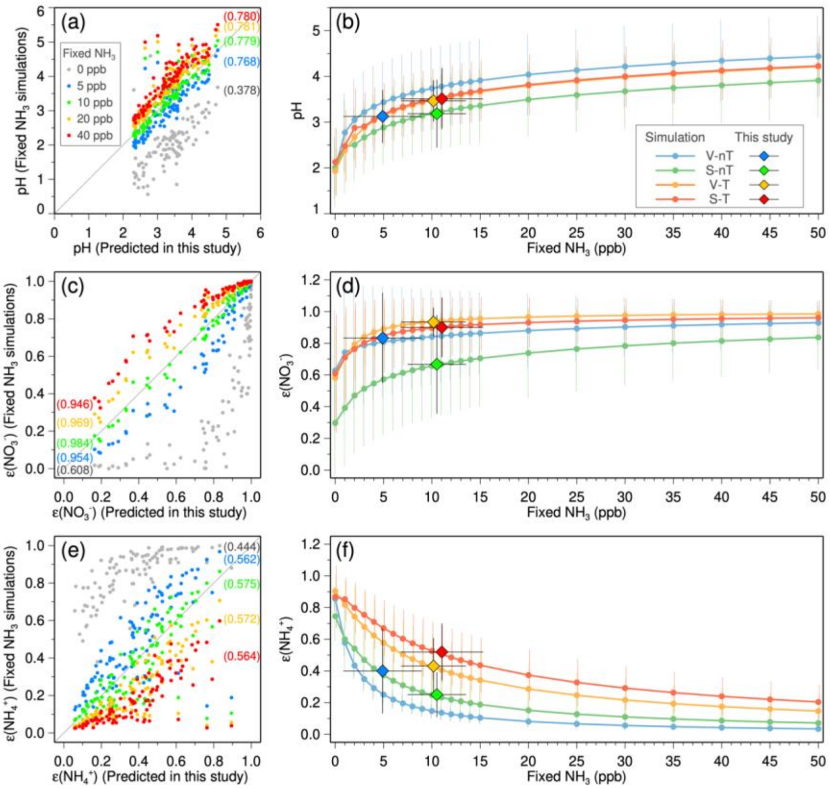

Figure 5: Sensitivity of (a–b) predicted pH, (c–d) nitrate partitioning ratio [$\varepsilon(NO_3^-) = NO_3^- / (HNO_3 + NO_3^-)$], and (e–f) ammonium partitioning ratio [$\varepsilon(NH_4^+) = NH_4^+ / (NH_3 + NH_4^+)$] to gas-phase ammonia ($NH_3$) concentrations. (a, c, and e) Comparisons between the simulation in this study (using the daily reconstructed NH_3 concentrations) and the simulations with the various fixed NH_3 levels (colored dots in gray, blue, green, yellow, and red for 0 ppb, 5 ppb, 10 ppb, 20 ppb, and 40 ppb, respectively). Values in round brackets are the R-squared values of the linear regressions. Gray solid lines indicate a 1-to-1 relationship. (b, d, and f) Average (solid circles) and standard deviation (vertical bars) of pH, $\varepsilon(NO_3^-)$, and $\varepsilon(NH_4^+)$ for the *local ventilation with no regional transport* (V-nT) group (light blue), *local stagnation with no regional transport* (S-nT) group (light green), *local ventilation with regional transport* (V-T) group (light yellow), and *local stagnation with regional transport* (S-T) group (light red) with respect to the various fixed NH_3 levels from 0 ppb to 50 ppb. Averages and standard deviations of the reconstructed NH_3 concentrations and obtained pH, $\varepsilon(NO_3^-)$, and $\varepsilon(NH_4^+)$ for the V-nT, S-nT, V-T, and S-T groups are represented as blue, green, yellow, and red diamonds with horizontal and vertical bars.

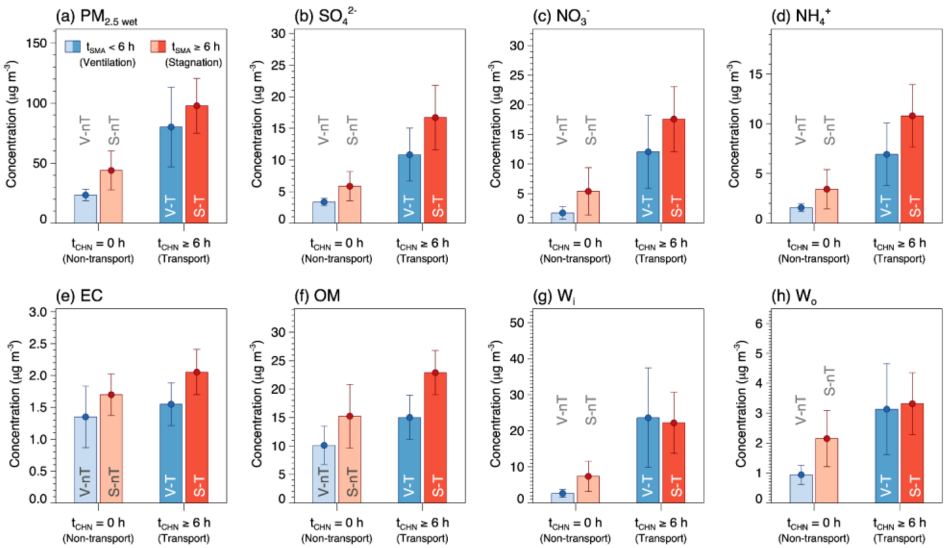

Figure 6: Average concentrations and confidence intervals at 95% of (a) wet $PM_{2.5}$ ($PM_{2.5\ wet}$), (b) sulfate (SO_4^{2-}), (c) nitrate (NO_3^-), (d) ammonium (NH_4^+), (e) elemental carbon (EC), (f) organic matter (OM), (g) inorganic ALW (W_i), and (h) organic ALW (W_o) for the *local ventilation with no regional transport* (V-nT) group (light blue), *local stagnation with no regional transport* (S-nT) group (light red), *local ventilation with regional transport* (V-T) group (darker light blue), and *local stagnation with regional transport* (S-T) group (darker light red) categorized by ranges of the average daily residence time of backward trajectories in the Seoul metropolitan area (t_{SMA}) and in the North China Plain and Yangtze River Delta (t_{CHN}).

삭제됨: SMA

삭제됨: NCP

삭제됨: YRD

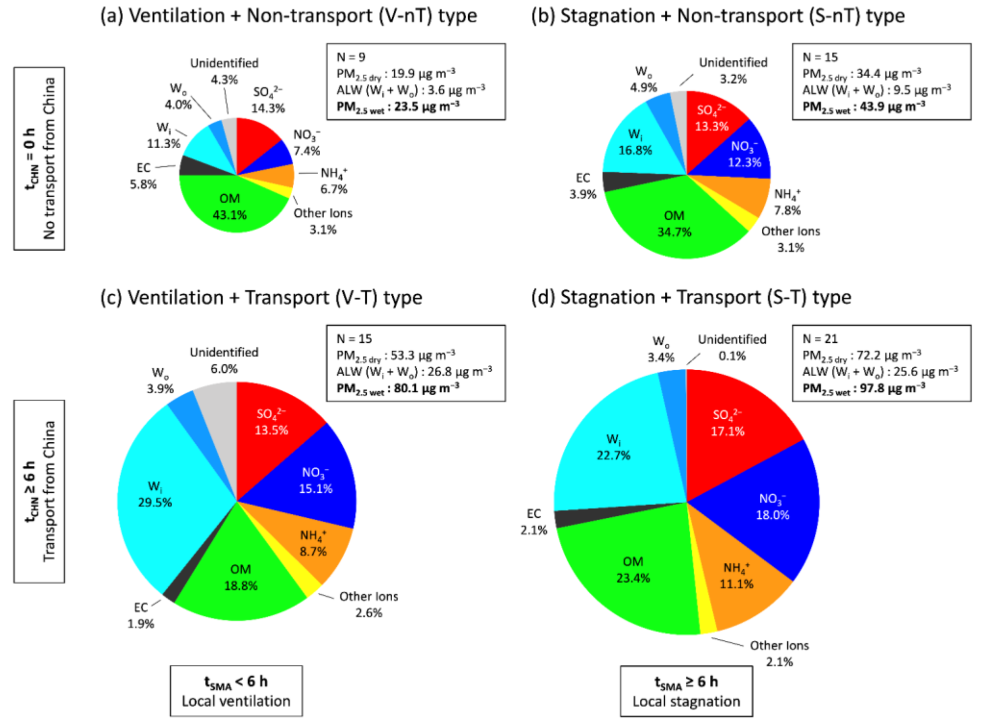

Figure 7: Average chemical compositions of wet $PM_{2.5}$ ($PM_{2.5\ wet}$) for the (a) *local ventilation with no regional transport* (V-nT) group, (b) *local stagnation with no regional transport* (S-nT) group, (c) *local ventilation with regional transport* (V-T) group, and (d) *local stagnation with regional transport* (S-T) group. Fractional species are sulfate (red), nitrate (dark blue), ammonium (orange), organic matter (green), elemental carbon (black), inorganic ALW (light blue), organic ALW (darker light blue), and other ions (chloride, sodium, potassium, magnesium, and calcium; yellow). The size of each circle is proportional to the $PM_{2.5\ wet}$ concentration.

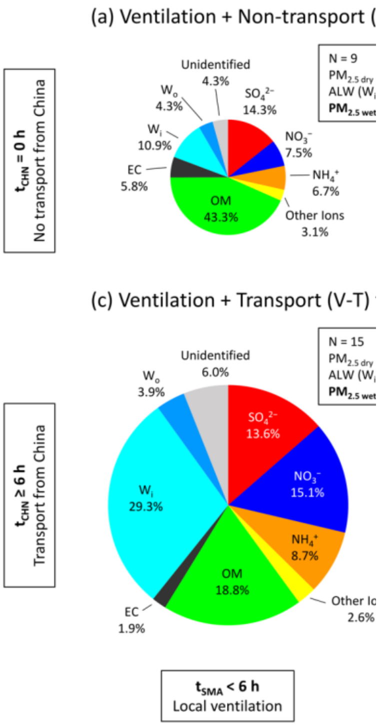

삭제됨:

삭제됨: 5

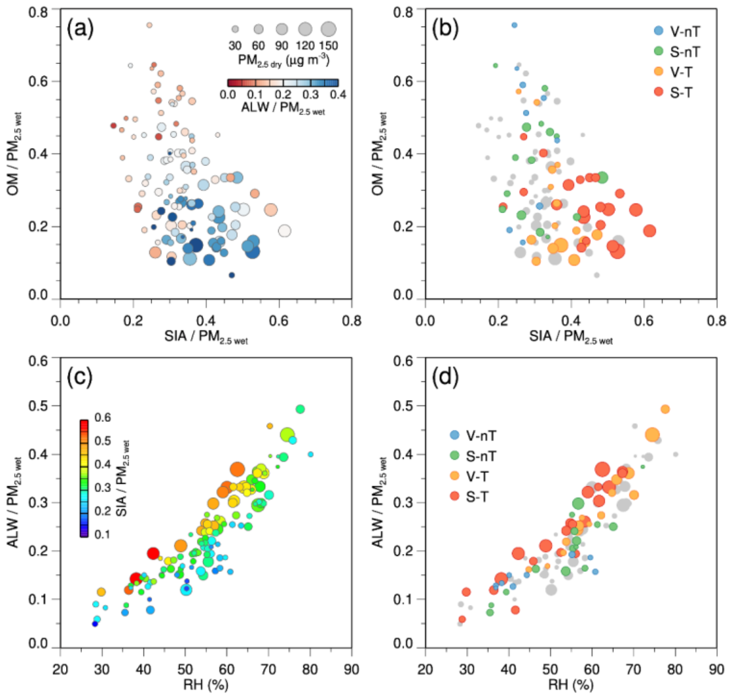

Figure 8: (a–b) Scatterplots of the secondary inorganic aerosol (SIA) fraction to wet PM$_{2.5}$ (SIA / PM$_{2.5\ wet}$) ratio versus the organic matter (OM) fraction to wet PM$_{2.5}$ (OM / PM$_{2.5\ wet}$) ratio, colored according to (a) the aerosol liquid water (ALW) to wet PM$_{2.5}$ (ALW / PM$_{2.5\ wet}$) ratio and (b) the categories for each case. (c–d) Scatterplots of ALW / PM$_{2.5\ wet}$ versus relative humidity (RH), colored according to (c) SIA / PM$_{2.5\ wet}$ ratio and (d) the categories. The size of each circle is proportional to the dry PM$_{2.5}$ (PM$_{2.5\ dry}$) concentration.

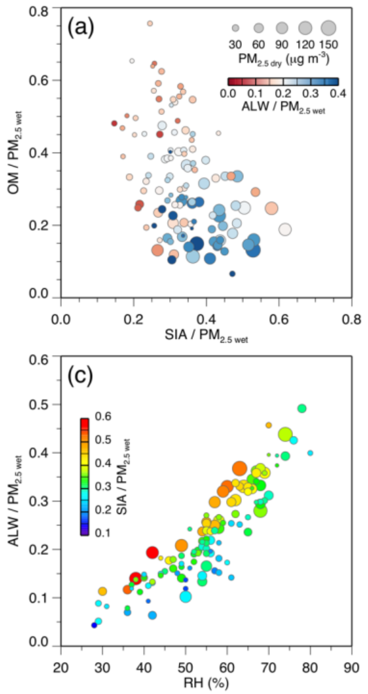

삭제됨:

삭제됨: 6

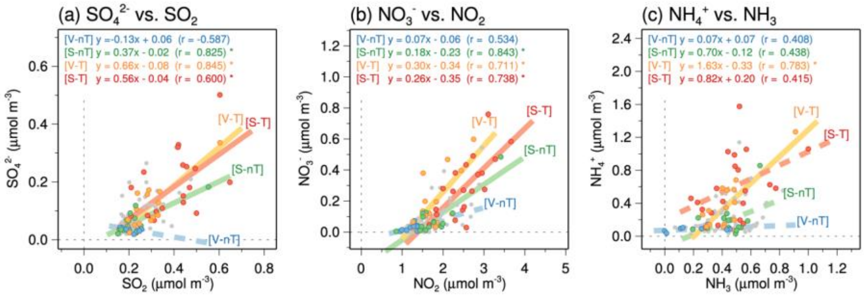

Figure 9: Scatterplots of (a) SO_4^{2-} versus SO_2, (b) NO_3^- versus NO_2, and (c) NH_4^+ versus the reconstructed ammonia (NH_3). Filled circles in blue, green, yellow, and red colors represent daily data belong to the *local ventilation with no regional transport* (V-nT) group, *local stagnation with no regional transport* (S-nT) group, *local ventilation with regional transport* (V-T) group, and *local stagnation with regional transport* (S-T) group, respectively. The statistically significant linear regression slopes ($p < 0.01$) for each group were represented by solid lines.

삭제됨: 7

삭제됨: represents

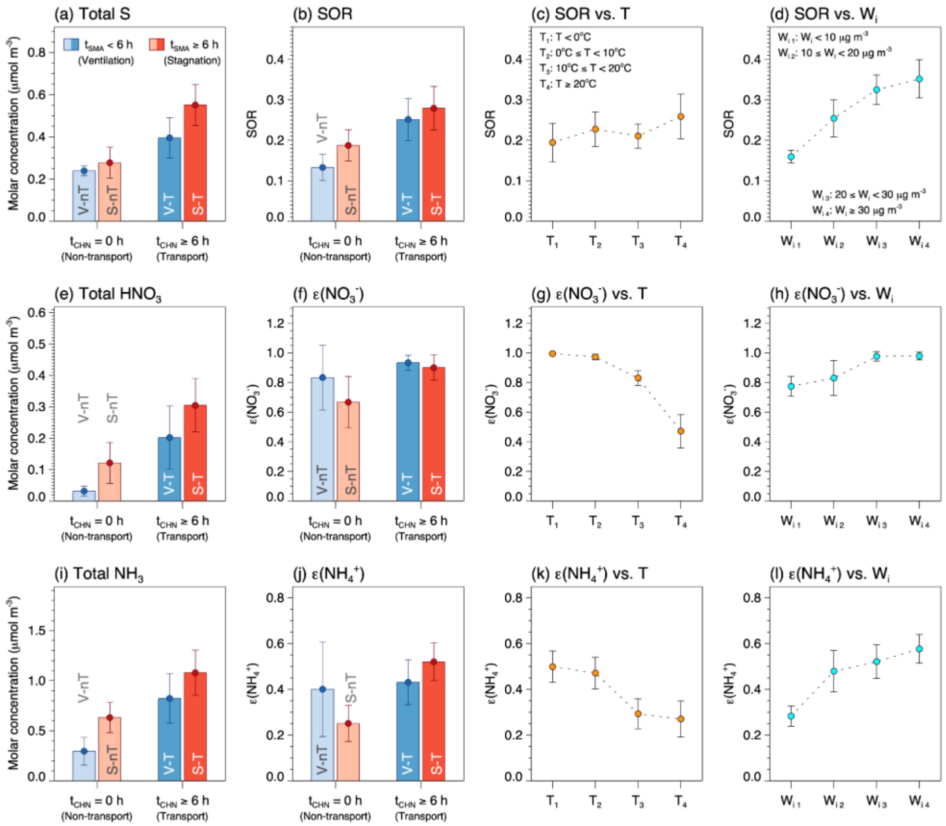

Figure 10: Average concentrations and confidence intervals at 95% of (a) total sulfur (= SO_2 + SO_4^{2-}), (b–d) sulfur oxidation ratio (SOR), (e) total HNO_3 (= HNO_3 + NO_3^-), (f–h) nitrate partitioning ratio [ε(NO_3^-)], (i) total NH_3 (= NH_3 + NH_4^+), and (j–l) ammonium partitioning ratio [ε(NH_4^+)]. (a–b, e–f, and i–j) Average for the *local ventilation with no regional transport* (V-nT) group (light blue), *local stagnation with no regional transport* (S-nT) group (light red), *local ventilation with regional transport* (V-T) group (darker light blue), and *local stagnation with regional transport* (S-T) group (darker light red). (c, g, and k) Average for the temperature (*T*) ranges of *T* < 0°C (T_1; *n* = 19), 0°C ≤ *T* < 10°C (T_2; *n* = 31), 10°C ≤ *T* < 20°C (T_3; *n* = 30), and *T* ≥ 20°C (T_4; *n* = 19). (d, h, and l) Average for the inorganic ALW (W_i) ranges of W_i < 10 μg m^{-3} (W_{i1}; *n* = 58), 10 μg m^{-3} ≤ W_i < 20 μg m^{-3} (W_{i2}; *n* = 14), 20 μg m^{-3} ≤ W_i < 30 μg m^{-3} (W_{i3}; *n* = 12), and W_i ≥ 30 μg m^{-3} (W_{i4}; *n* = 15).

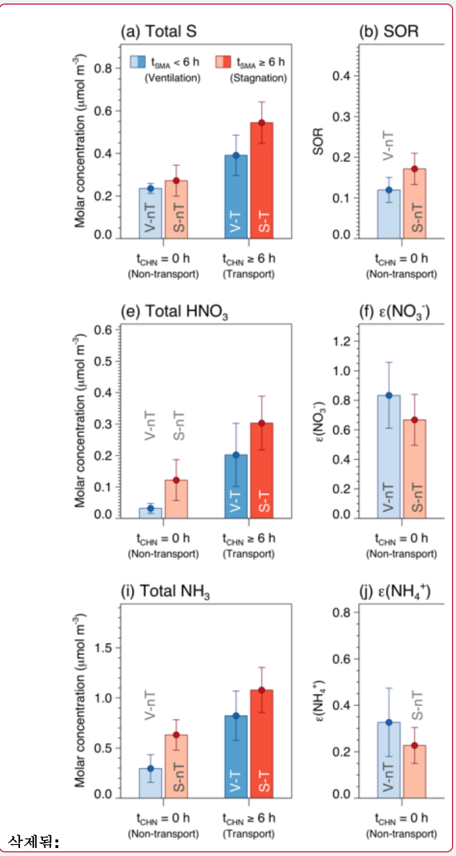

삭제됨:

삭제됨: 8

삭제됨: (

삭제됨: $^-$)),

삭제됨: (

삭제됨: $^+$)).

삭제됨: 60

삭제됨: 12

삭제됨: 13

삭제됨: 14

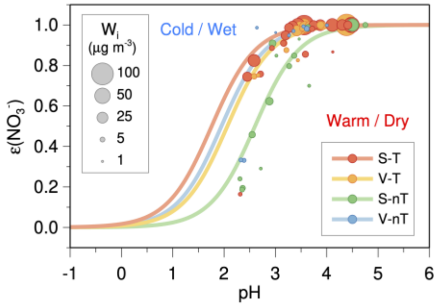

Figure 11: The calculated sigmoid curves (S-curves) and observed ambient gas-particle partitioning ratios (solid circles) for nitrate $[\varepsilon(NO_3^-)]$ plotted against the ISORROPIA-predicted particle pH. The blue, green, yellow, and red circles represent the *local ventilation with no regional transport* (V-nT) group, *local stagnation with no regional transport* (S-nT) group, *local ventilation with regional transport* (V-T) group, and *local stagnation with regional transport* (S-T) group, respectively, and the size of each circle is proportional to the concentration of inorganic ALW (W_i). The curves were calculated based on the median values of temperature (T), W_i, and product of activity coefficient ($\gamma_{H^+}\gamma_{NO_3^-}$) for each group; T = 0.6°C, W_i = 2.2 μg m^{-3}, and $\gamma_{H^+}\gamma_{NO_3^-}$ = 0.146 for the V-nT group; T = 17.5°C, W_i = 5.6 μg m^{-3}, and $\gamma_{H^+}\gamma_{NO_3^-}$ = 0.295 for the S-nT group; T = 11.6°C, W_i = 16.6 μg m^{-3}, and $\gamma_{H^+}\gamma_{NO_3^-}$ = 0.458 for the V-T group; T = 6.9°C, W_i = 18.0 μg m^{-3}, and $\gamma_{H^+}\gamma_{NO_3^-}$ = 0.400 for the S-T group.

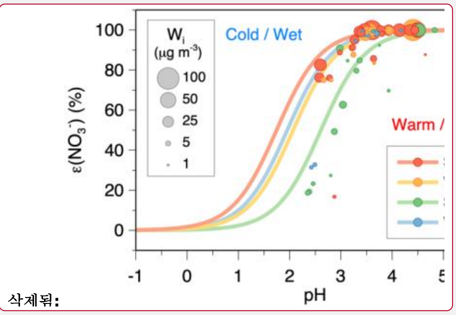

삭제됨:

삭제됨: 9

삭제됨: (

삭제됨: ⁻))

삭제됨: 150

삭제됨: 4

삭제됨: 293

삭제됨: 5

삭제됨: 459

삭제됨: 4

삭제됨: 397

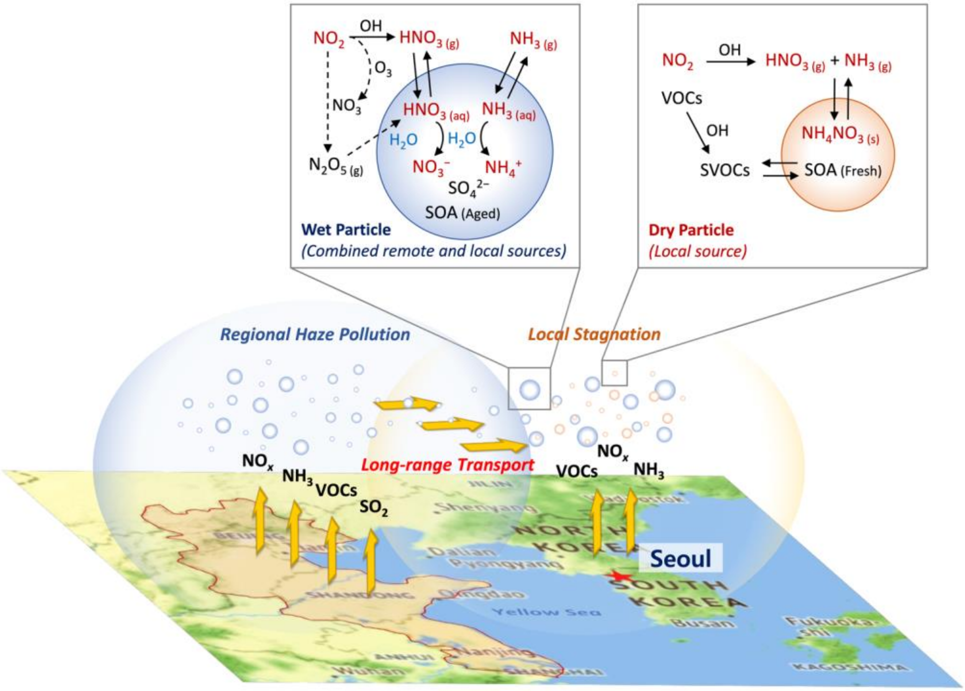

Figure 12: Schematic of synergistic nitrate partitioning to the particle phase aided by wet particles transported from the remote source area (North China Plain and Yangtze River Delta) in a high NO_x and NH_3 urban area (Seoul metropolitan area) during the cold season in East Asia. The background map was derived from © Google Maps.

삭제됨: 10

삭제됨: NCP

삭제됨: YRD